Bachelors Thesis

Characterization of Continuum Gas Flow in a High-Pressure
Micro-Reactor Assembly

Vienna University of Technology

Institute of Applied Physics

under guidance of

Ing. Adam Lagin
Dr.techn. Jiri Pavelec
Univ.Prof. Gareth Parkinson PhD

submitted by

Martin Kronberger
Matr.-Nr.: 12202316

Author:
Martin Kronberger

Supervisor:
Univ.Prof. Gareth Parkinson PhD

1 May 2025

Declaration of Authorship

Martin Kronberger

I hereby declare that I have written this thesis independently and that I have fully acknowledged all the sources and aids used. Furthermore, I confirm that I have marked as borrowed any parts of this work (including tables, maps, and figures) that are taken from other works or from the internet, either verbatim or in spirit, giving explicit reference to the source.

I further declare that large language models were used solely to assist with formatting, providing code snippets, and helping to resolve minor technical issues. These models did not contribute to the research content, analyses, interpretations, conclusions, or any intellectual substance of this thesis.

_____

Martin Kronberger
Vienna, 1 Mai 2025

Acknowledgements

Danksagung

Zuallererst möchte ich Adam Lagin meinen tief empfundenen Dank aussprechen, dessen Doktorarbeitsprojekt zur Entwicklung einer Hochdruckzelle die Grundlage und Motivation für diese Arbeit bildete. Seine kontinuierliche Unterstützung, wertvollen Diskussionen und hilfreichen Ratschläge haben maßgeblich zur Verfeinerung und Fertigstellung meiner Forschung beigetragen. Besonders dankbar bin ich außerdem für die vielen gemeinsamen Kaffeepausen, die mir halfen, den Kopf freizubekommen und den Überblick zu bewahren.

Weiterhin möchte ich mich herzlich bei Jiri Pavelec für seine geduldige und sorgfältige Betreuung bedanken, insbesondere hinsichtlich der Struktur sowie der Ziele und des Umfangs dieser Arbeit. Seine klaren Ratschläge und seine Geduld haben meine Arbeit wesentlich verbessert.

Schließlich gilt mein aufrichtiger Dank meinen Physikprofessoren Franz Klammler und Wilfried Burgstaller, deren hervorragende Lehre meine Neugier und Begeisterung für die Physik geweckt und meinen Entschluss gestärkt hat, den Weg zum Physiker einzuschlagen.

Abstract

Understanding catalytic processes at the atomic scale under realistic conditions is a key challenge in surface science. In particular, the study of single-atom catalysis at near-ambient pressures requires specialized experimental setups, such as high-pressure micro-reactor cells integrated into ultra-high vacuum (UHV) systems. This thesis develops an analytical framework to describe gas flow behavior within such a micro-reactor, focusing on the continuum flow regime. Critical state variables and flow velocities at relevant locations are estimated to provide a reliable macroscopic flow description. While effects such as leakage and outlet flow remain to be quantified in detail and should incorporate advanced numerical simulations and experimental validation to improve the model accuracy and applicability. The presented approach lays the groundwork for future microscopic flow studies.

Kurzfassung

Das Verständnis katalytischer Prozesse auf atomarer Ebene unter realistischen Bedingungen stellt eine zentrale Herausforderung in der Oberflächenwissenschaft dar. Insbesondere die Untersuchung der Einzelatomkatalyse bei nahezu Umgebungsdruck erfordert spezialisierte experimentelle Aufbauten, wie Hochdruck-Mikroreaktorzellen, die in Ultrahochvakuum-(UHV)-Systeme integriert sind. Diese Arbeit entwickelt einen analytischen Rahmen zur Beschreibung des Gasströmungsverhaltens innerhalb eines solchen Mikroreaktors, mit Fokus auf das Kontinuumsströmungsregime. Kritische Zustandsgrößen und Strömungsgeschwindigkeiten an relevanten Stellen werden abgeschätzt, um eine verlässliche makroskopische Strömungsbeschreibung bereitzustellen. Effekte wie Leckagen und der Auslassstrom müssen hingegen noch im Detail quantifiziert werden und sollten durch weiterführende numerische Simulationen und experimentelle Validierung in das Modell integriert werden, um dessen Genauigkeit und Anwendbarkeit zu verbessern. Dennoch bildet der vorgestellte Ansatz die Grundlage für zukünftige mikroskopische Strömungsuntersuchungen.

Contents

Introduction

Catalysis is an inseparable part of modern society, relying on the chemical industry, solutions in ecology, or effective energy storage. Therefore, the development of superior catalysts has been in the scope of surface science for many years.

One of the approaches is the preparation and investigation of model catalysts in the form of single-crystal support with well-defined active sites. The use of inexpensive support materials and the reduction of deposited noble metals significantly increase the effectiveness and selectivity of model catalysts. Such a catalyst configuration also enables a better understanding of physical processes happening on its surface.

However, their preparation and investigation require ultra-high vacuum (UHV) to preserve adequate inertness of the surrounding environment. Therefore, the laboratory pressure conditions usually do not reflect the real industrial setup. To bridge this pressure gap, the microreactor (high-pressure cell) located in the UHV chamber, enabling sample exposure to elevated gas pressure and temperature, is under development.

There are several similar devices in use, however, their microscopic flow description is often trivialized. And particularly flow conditions at the reactive surface have a significant influence on the reactant and product transportation. Omitting these factors can then result in a misleading read of the catalytic activity.

The main scientific task is to get an uncomplicated and reliable overview of the macroscopic gas flow properties inside the high-pressure cell located in the UHV chamber. The appropriate gas flow theory is presented initially and later applied to certain geometry and required conditions. The main attention was paid to selected, most-critical locations in the micro reactor. The obtained results, respectively the formulated approach to calculate gas properties, are essential for ongoing microscopic flow investigation, and can be easily applied on adjusted geometry of high-pressure cells.

1 Scope and objectives

The aim of this thesis is to develop a straightforward analytical framework that predicts gas flow behavior and estimates key state variables at strategically relevant positions within a micro-reactor assembly. These state variables include pressure, temperature, density, and flow velocity, which together provide a macroscopic description of the system's thermodynamic and transport conditions. Accurate knowledge of these parameters is essential for understanding the overall flow dynamics and for defining reliable boundary and initial conditions for subsequent numerical simulations of microscopic or reactive flow phenomena.

Figure 1 illustrates the reactor configuration. Reactants are first introduced into the reservoir, where they mix before entering the reaction zone through a narrow inlet. Within the reaction volume, gas molecules interact with the active surface of the sample under controlled conditions. The flow then continues through the outlet into the ultra-low-pressure analysis section, where residual gases are removed. In parallel, a small fraction of the gas leaks through the sealing interface into the sample transfer section of the surrounding vacuum chamber, affecting local pressure distributions.

This model focuses on the continuum flow regime and provides estimates of state variables at critical locations such as the reservoir, inlet, reaction chamber, outlet, and leak path. These estimates form the foundation for assessing flow behavior under near-ambient pressures and will later be refined by high-resolution numerical methods and experimental validation.
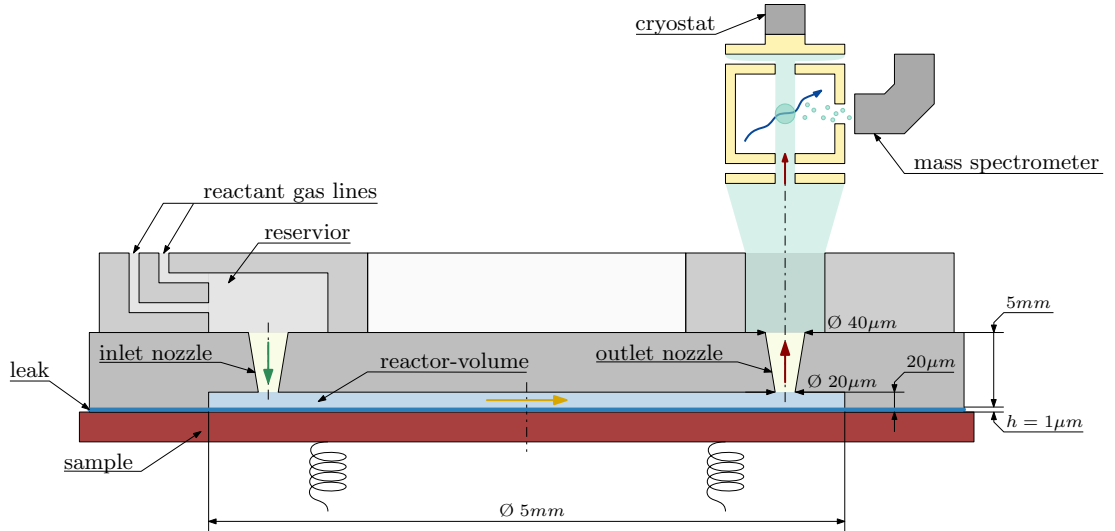
Figure 1. Schematics of the micro-reactor assembly [1]: The reactants are mixed in the reservoir, pass progressively through the inlet (green arrow), reaction volume (yellow arrow), and exhaust into the vacuum through the outlet (red arrow). The exhaust gas composition is analyzed via quadrupole mass spectroscopy. The part of the gas in the reaction volume leaks through the space between the sample and the sealing surface of the reactor (blue line).

The sections that follow, address four main objectives: identifying the dominant flow regime, quantifying the impact of leakage, characterizing the gas state close to the sample, and predicting some characteristics of the velocity distribution at the outlet. To achieve these goals, the analysis relies on established concepts such as the Knudsen and Reynolds numbers, along with one-dimensional isentropic flow theory. This foundation, which is detailed in the subsequent chapter on foundational principles, not only clarifies the interaction between the reactor's geometry and gas dynamics but also lays the groundwork for future numerical simulations and experimental studies.

1.1 Type of Flow

The type of flow has major implications on which mathematical formulations and simulations are applicable, as well as the way the gas particles interact with each other and the walls of the assembly. The main focus here is on the *Knudsen number* and the idealized flow regimes connected to it. With the main goal being to assess the most likely flow regime governing the inside of the assembly and therefore determine the equations applicable to calculate the state variables at different points in the system and the throughput of the system as a whole.

In preparation for numerical simulations it is also important to find a way to calculate Knudsen numbers and other flow parameters using given datasets of state variables without having to rely on flow regime specific methods. This will help to analyze transient regimes, encountered when the gas expands into the vacuum, using generally applicable methods.

1.2 Impact of the leak

As described in the introduction of this chapter, there will be some leakage expected at the boundary between the reactor casing and the sample. This leak will inevitably lead to additional mass-flow and therefore a pressure drop ΔP_L inside the reactor. This can lead to major changes to the steady state of the system, therefore influencing the gas-flow into the reactor just as the velocity distribution at the outlet. In summary the goal is finding the maximum mass flow $\dot{m}_L$ caused by the leak, which would result in sonic speeds at the inlet throat, resulting in undefined behavior inside the micro reactor, like sudden changes in state variables in the form of shockwaves.

1.3 Behavior of the gas around the sample

Knowing more about the state the gas is in close to the sample is very helpful. These can be used to estimate values for diffusion rates to and from the surface, boundary layer thickness, and mean velocities and momentum of particles reaching the reactive surface. Important metrics are the velocity, pressure and temperature of the gas and the type and behavior of flow.

1.4 Velocity distribution at the outlet

After the gas leaves the outlet nozzle, it expands into a vacuum chamber where the gas atoms reach the ionizer and once ionized can get analyzed by the quadrupole mass spectrometer (QMS), to measure the ratio of different products. This won't be the case for all atoms, since for an atom to be ionized it has to cross the ionization area, which is localized in space. The remaining gas has to be pumped out of the vacuum chamber and doesn't contribute to the ratio measured by the mass-spec. Therefore, it is important to approximate, how much of the gas leaving the outlet actually is able to reach the region of influence of the electron beam and will contribute to the measurement of the QMS. To answer this the velocity distribution of the expansion after the gas is fully rarefied is needed. This distribution can then essentially be treated as a source like surface, with no interaction between gas particles after this point, and can therefore be directly correlated to the amount of atoms reaching the sphere of influence of the electron beam.
Knowing what determines the distribution of the outlet can also help identify changes to be made to the geometry or the reservoir conditions to increase the amount of atoms reaching the QMS.

2 Foundational Principles

When dealing with advanced fluid or gas dynamical systems, they must first be categorized before suitable models can be formulated. This is typically done by determining dimensionless numbers whose values characterize the behavior of the gas and its interaction with its surroundings. Essentially, the values of these dimensionless numbers indicate which theoretical formulations are applicable and whether additional boundary conditions or considerations must be accounted for. This first chapter will detail the calculation of several key dimensionless numbers and discuss their implications for model selection and applicability.

2.1 Characteristic Length and Wetted Perimeter

The characteristic length L_c essentially serves the purpose of scaling physical systems. It is fundamental when calculating most dimensionless quantities especially, if these are connected to the scale of the system. Therefore, these quantities usually dependent on the characteristic length scale of the system or parts of the system, to be able to describe the geometry abstractly.
For internal flows the characteristic length is defined as:

$$L_c = \frac{4A}{P_w} \quad \text{with} \quad P_w = \sum_{i=0}^{\infty} l_i \tag{2.1}$$

Where A is the cross-sectional area and P_w is the wetted perimeter, which is defined as the sum over the length of edges in the cross-section in direct contact with the fluid. For gaseous fluids the whole perimeter of the cross-section must be considered, therefore the wetted perimeter reduces to the perimeter of the cross-section. The following section provides the characteristic length formulas for common duct shapes. [2]

circular duct   rectangular duct

$$P_{w,\,circ} = \pi D \quad \rightarrow \quad L_{c,\,circ} = D \qquad P_{w,\,rect} = 2H + W \quad \rightarrow \quad L_{c,\,rect} = \frac{2HW}{H+W}$$
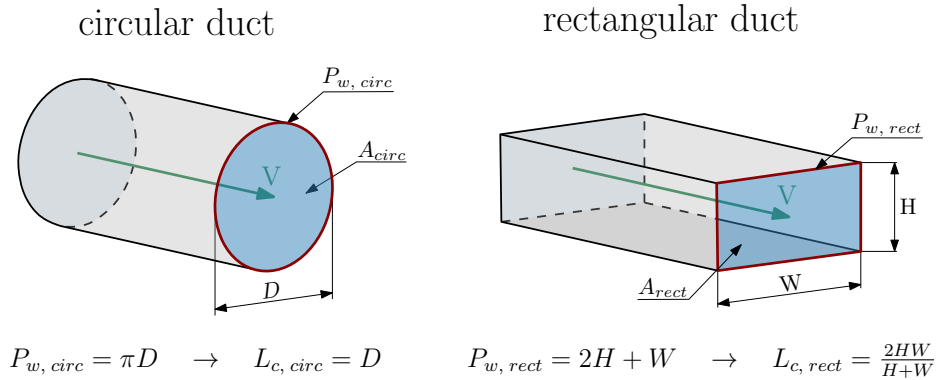
If the height H of a rectangular duct is very small compared to its width W, it is more convenient to view it as an asymptotic case where the width approaches infinity $(W \to \infty)$.

two parallel plates

$$L_{c,\,plates} = \lim_{W \to \infty} L_{c_\square} = \lim_{W \to \infty} \frac{2HW}{H+W} = 2H$$
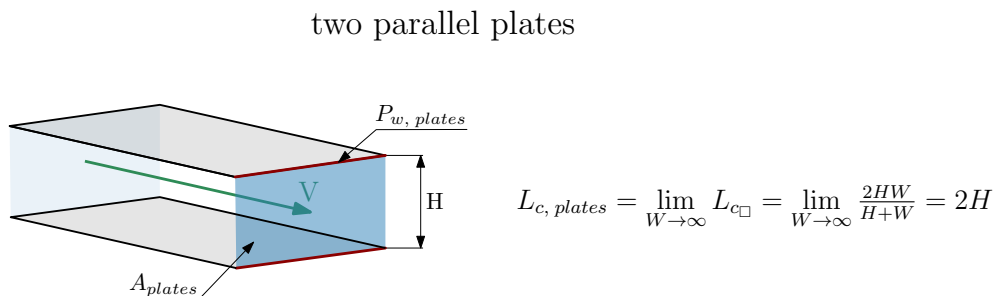
2.2 Turbulence and the Reynolds number

To categorize the qualitative movement of a fluid, specifically whether it exhibits smooth, layered motion or chaotic, fluctuating behavior, the Reynolds number is introduced as a dimensionless quantity characterizing the ratio of inertial to viscous forces. This quantity is defined as:

$$\mathrm{Re} = \frac{\rho V L_c}{\mu(T)} = \frac{V L_c}{\nu} \tag{2.2}$$

Where ρ is the fluid density, V is the flow speed, L_c is a characteristic length (such as pipe diameter as described in Section 2.1), μ is the dynamic viscosity, and ν is the kinematic viscosity. These flow behaviors can be sorted into three categories depending on the value of the Reynolds number: [3, 4]

- Laminar flow Re < 2000: where fluid moves in smooth layers, with minimal mixing between those layers.

- Transitional flow $2000 \geq \mathrm{Re} \geq 4000$: marks the transition between the main regimes.

- Turbulent flow Re > 4000: where the fluid moves chaotic and mixes irregularly due to formation of eddies.

2.3 Rarefaction and the Knudsen number

In fluid dynamics a flow can also be categorized by its particle interaction using the Knudsen number, which represents the ratio between the mean-free-path λ of the gas and the characteristic length L_c of the flow geometry.

$$\mathrm{Kn} = \frac{\lambda}{L_c} = \frac{\mu(T)}{p\,L_c} \sqrt{\frac{\pi\,T\,R_u}{2\,M_m}}, \tag{2.3}$$

Molecular regime ($\mathrm{Kn} \geq 10$)

In this regime, the mean free path λ is much larger than the distance between boundaries. This leads to particle interactions themselves becoming negligible in comparison to the interaction of particles with the boundary.
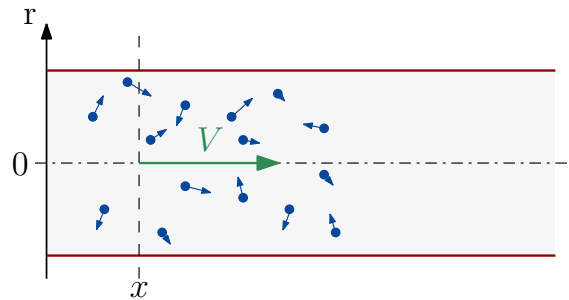
Figure 2. Schematic of particle velocities at a cross-section in a circular duct under molecular flow conditions: The red lines denote the duct boundaries, the green arrow and line represent the mean velocity at position x, blue dots and arrows represent individual particles and their velocity.

Transition regime $(0.1 \leq \text{Kn} \leq 10)$

This regime constitutes the middle ground between continuum and molecular flow. Neither the continuum assumptions of fluid dynamics nor the free molecular flow assumptions hold completely. The interactions between the gas molecules and the boundaries become significant, and the flow characteristics may vary widely. The transition between continuum and molecular flow is commonly referred to as rarefaction, with fully developed molecular flow being classified as rarefied flow.

Slip regime $(0.001 \leq \text{Kn} \leq 0.1)$

For increasing Knudsen numbers, the mean free path of the gas molecules becomes comparable to the characteristic length scale of the system. In this regime, the assumptions of continuum flow still largely hold, but noticeable deviations arise, particularly near the boundaries. While continuum mechanics assumes a strict no-slip condition at the boundary, in this transitional regime, a finite slip velocity must be considered. This effect is associated with the presence of a Knudsen layer — a thin region adjacent to the boundary where molecular collisions and wall interactions cause non-equilibrium behavior, leading to a breakdown of the continuum assumption.
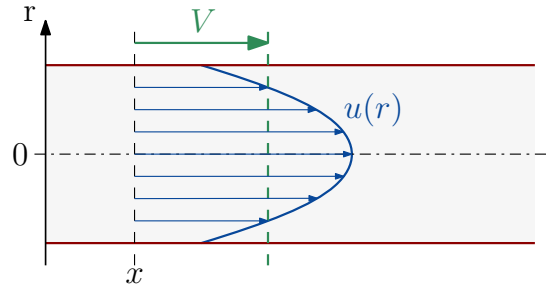
Figure 3. Schematic of the velocity distribution at a cross-section in a circular duct under slip flow conditions: The red lines indicate the duct boundaries, the green arrow and line denote the mean velocity at position x, and the blue function with arrows shows the velocity profile modified by slip effects at the walls. [3]

Continuum regime $(\text{Kn} \leq 0.001)$

As the characteristic length starts to become much larger than the mean free path of the gas, the interactions of particles in the medium are much more frequent than the interactions of particles with the boundaries of the duct. This makes it possible to describe the fluid itself as a continuous medium with the assumption of non-slip boundary conditions. The Navier-Stokes equations govern the calculations in this regime.
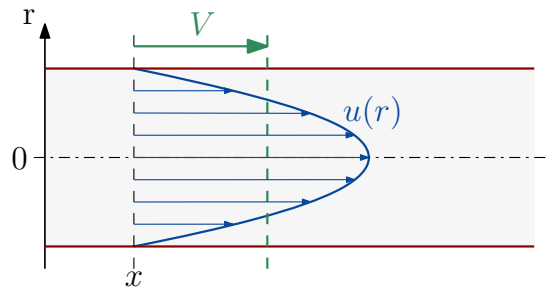
Figure 4. Schematic of the velocity distribution at a cross-section in a circular duct under continuum flow conditions: The red lines mark the duct boundaries, the green arrow and line indicate the mean velocity at position x, and the blue curve with arrows represents the classical velocity profile typical of fully developed laminar flow. [3]

In this work the continuum formulations will be used exclusively, with the reasons more clearly described in Section 3.2. [5, 6, 7, 2]

2.4 Sutherland's Law

A key aspect when calculating dimensionless numbers like Knudsen number (Section 2.3) and Reynolds number (Section 2.3) is capturing the temperature dependence of the dynamic viscosity. For this purpose, Sutherland's law is used to express the dynamic viscosity $\mu(T)$ as

$$\mu(T) = \mu_{\mathrm{ref}} \left(\frac{T}{T_{\mathrm{ref}}} \right)^{3/2} \frac{T_{\mathrm{ref}} + S_\mu}{T + S_\mu}, \tag{2.4}$$

where μ_{ref}, T_{ref}, and S_μ are empirical constants. This formulation provides a reasonable approximation for many gases within a broad temperature range.

2.5 Dimension of the flow

The dimension of the flow describes the number of positional parameters needed to yield an exact solution for a given flow velocity field $V(\vec{x})$, so equals essentially $\dim(\vec{x})$. The flow through a constant area duct is usually described using a one-dimensional flow field only depending on the position x along the length of the duct. In the case of more complicated geometries the flow must be described using a three-dimensional velocity field, thus depends on all spatial coordinates. In the case of variable area ducts – like nozzles and diffusers – assuming only a slight change in area along the length of the duct the flow can be approximated using a one-dimensional flow field with enough precision. This is called quasi one-dimensional flow. [4]

2.6 Isentropic one-dimensional flow

Isentropic, quasi one-dimensional, varying-area flow is one of the most idealized models used to describe the behavior of gases flowing through confined geometries. To simplify the analysis and make the governing equations solvable in a straightforward way, several assumptions are applied:

- **Steady, one-dimensional flow**
  Flow properties vary only along the direction of flow.

- **Adiabatic conditions**
  No heat exchange with the surroundings is considered ($\delta q = 0, ds_e = 0$).

- **No external work input**
  No mechanical work is performed on the system ($\delta w_s = 0$).

- **Negligible change in potential energy**
  Elevation differences are assumed insignificant ($dz = 0$).

- **Reversible process**
  No internal entropy change occurs ($ds_i = 0$).

These simplifications imply that the flow is isentropic, meaning both adiabatic and reversible. This allows the use of analytical relations to describe the flow behavior and connect the state variables along the flow path. The gas is still considered perfect and follows the perfect gas law, as it is crucial in the derivation for the following relations which are the foundation for solving isentropic one-dimensional gas flows.

Flow velocity for continuum flows is usually encoded into the Mach number, which is defined as the ratio between the flow velocity V and the local speed of sound a. Which can be calculated using the ratio of heats γ and the temperature T of the gas and the specific gas constant R. It describes the speed at which small pressure disturbances propagate through the gas.

$$\text{Ma} = \frac{V}{a} \quad \text{where} \quad a = \sqrt{\gamma R T} \tag{2.5}$$

It is a very important metric when analyzing isentropic flow, since state variables are uniquely defined through the mach number at the corresponding location, as long as either the stagnation, or critical conditions of the flow are known. For isentropic flow one-dimensional flow it can be directly linked to the geometry of the duct and can be calculated by defining a state in the system where Mach number is equal to 1, the so-called throat. Then its area can be related to the Mach number by following non-linear equation:

$$\frac{A}{A^*} = \frac{1}{\text{Ma}} \left[\frac{2}{\gamma + 1} \left(1 + \frac{\gamma - 1}{2} \text{Ma}^2 \right) \right]^{\frac{\gamma+1}{2(\gamma-1)}} \tag{2.6}$$

where A is the local cross-sectional area, A^* the throat area (minimum cross-section), Ma the Mach number at the given location, and γ the specific heat ratio.

One of the most important ideas in isentropic flow are the stagnation/total conditions, which represent the state of a moving gas when fully decelerating it isentropically (Ma = 0). They exist for the fundamental state variables of the gas notated as (P_0, T_0, ρ_0) and represent conserved quantities when dealing with isentropic flow. This stagnation state does not have to exist in the system, but can be derived if state variables and the geometry at some point in the system are known. Total conditions represent the highest values for any state variable in the system other than velocity, as long as the flow stays isentropic. Therefore, changes of state variables are usually represented in relation to the total conditions of the corresponding state variables, and depend only on the ratio of heats of the gas γ and the Mach number Ma.

$$\frac{T}{T_0} = \left(1 + \frac{\gamma - 1}{2} \text{Ma}^2 \right)^{-1} \tag{2.7}$$

$$\frac{p}{p_0} = \left(1 + \frac{\gamma - 1}{2} \text{Ma}^2 \right)^{-\frac{\gamma}{\gamma-1}} \tag{2.8}$$

$$\frac{\rho}{\rho_0} = \left(1 + \frac{\gamma - 1}{2} \text{Ma}^2 \right)^{-\frac{1}{\gamma-1}} \tag{2.9}$$

Low subsonic regime (Ma < 0.3)   For low Mach numbers, compressibility effects of a gas can be neglected, and the gas can be treated as an incompressible fluid. In the figures, regions where the flow is expected to have very low Mach numbers are indicated by yellow arrows (as shown in Figure 1).

Subsonic regime (0.3 < Ma < 1.0)   Inside system of variable area ducts the gas flow generally stays subsonic. Once sonic speed is reached in a converging duct, the behavior reverses, and the velocity decreases, limiting the flow to subsonic or sonic speeds within purely converging ducts. In the figures, regions where the flow is expected to be subsonic are indicated by green arrows (as shown in Figure 1).

subsonic nozzle   subsonic diffuser
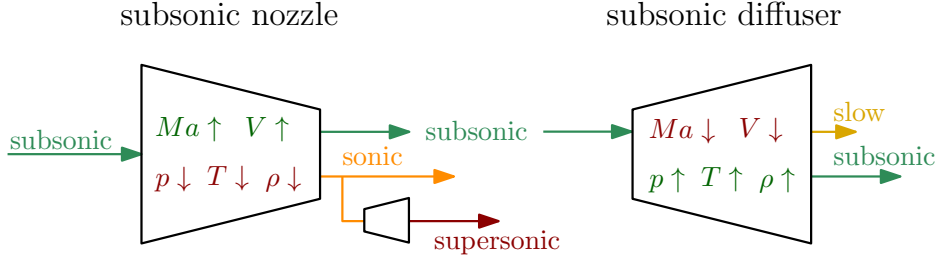
Figure 5. Schematic illustrating changes in state variables for subsonic flow in a converging nozzle (left) and a diverging diffuser (right): Colored arrows indicate possible flow regimes: green for subsonic flow, orange for sonic flow, red for supersonic flow, and yellow for slow subsonic flow. In the nozzle, Mach number and velocity increase while pressure, temperature, and density decrease. Conversely, in the diffuser, Mach number and velocity decrease, and pressure, temperature, and density rise. Additionally, the schematic shows that supersonic flow can only be achieved if the flow first passes through a sonic condition (choked flow) at the nozzle throat. [3]

Sonic regime ($\mathrm{Ma} = 1$) Sonic flow occurs at the exit of a converging duct when the pressure ratio between the upstream and downstream reservoirs drops below a certain critical value. This condition is referred to as *choked flow* and represents the maximum possible mass flow rate for the given stagnation conditions. The corresponding critical pressure ratio is defined as:

$$\frac{P^*}{P_0} = \left(\frac{2}{\gamma + 1}\right)^{\frac{\gamma}{\gamma - 1}} \tag{2.10}$$

where P_0 is the stagnation pressure, P^* the critical back pressure, and γ the ratio of specific heats.

Once the flow becomes choked at the throat, any further decrease in back pressure does not affect the mass flow rate but causes the flow to accelerate beyond the throat, leading to supersonic conditions in the diverging section. The critical pressure ratio can be derived from the isentropic flow relations (see Equation (2.7)) and can equivalently be expressed in terms of other thermodynamic variables, as summarized in the formulary.

Supersonic regime ($\mathrm{Ma} > 1$) If there are critical conditions at the end of a converging duct and a diverging duct follows. The flow continues to accelerate and reaches supersonic speeds. The location where the flow reaches critical condition is called throat and represents the minimal diameter of the duct.
In supersonic flows, state variables change rapidly causing phenomenons like shock waves and expansion fans. Just like for previous regimes, this regime will be indicated using an arrow colored red. [8]
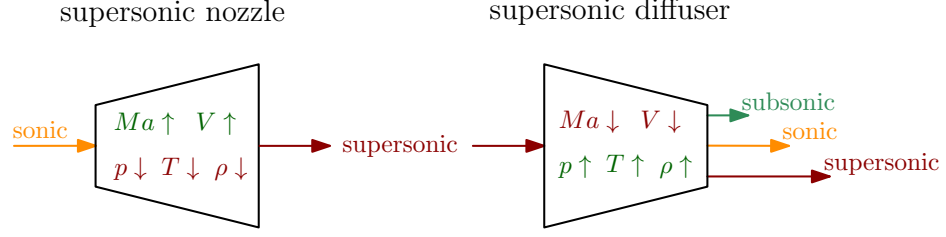
Figure 6. Schematic illustrating changes in state variables for supersonic flow in a diverging nozzle (left) and a converging diffuser (right): Colored arrows indicate different flow regimes: orange for sonic flow, red for supersonic flow, and green for subsonic flow. In the nozzle, Mach number and velocity increase while pressure, temperature, and density decrease. Conversely, in the diffuser, Mach number and velocity decrease, and pressure, temperature, and density rise. Supersonic flow can only be established if the flow first reaches sonic conditions at the throat, followed by further expansion. [3]

Mass flow   Mass flow is conserved along the flow and can be calculated using following equation, which derives from the equation for mass-flow in a steady one-dimensional flow (2.11), the isentropic relations [Equations (2.7) - (2.8)] and the ideal gas law. [9]

$$\dot{m} = A \cdot P_0 \cdot \sqrt{\frac{\gamma M_m}{T_0 R_u}} \cdot \mathrm{Ma} \cdot \left(1 + \frac{\gamma - 1}{2} \mathrm{Ma}^2\right)^{-\frac{\gamma+1}{2(\gamma-1)}} \tag{2.11}$$

Relation of dimensionless numbers in continuum flow   It is possible to relate the three dimensionless numbers mentioned in the preceding chapters. Leading to following relation:

$$\mathrm{Kn} = \frac{\mathrm{Ma}}{\mathrm{Re}} \sqrt{\frac{\gamma \pi}{2}} \tag{2.12}$$

Where Ma is the Mach number, Re the Reynolds number and Kn the Knudsen number at some point along the flow of gas with the ratio of heat γ. [3, 10, 11]

3 Analytical work

Now that the fundamental principles have been established, this chapter focuses on addressing the key questions outlined in Chapter 1. First, the geometry of the assembly is defined more rigorously to enable the determination of characteristic lengths and cross-sectional areas at all relevant locations. Additionally, the conditions within the reservoir and the vacuum environment are specified, as they significantly influence the resulting flow behavior.

Subsequently, the expected flow regimes are discussed to verify whether the isentropic continuum flow model introduced earlier is applicable. These assumptions will then be validated through analytical calculations. As a starting point, the assembly is approximated as a variable-area duct without leakage, allowing the application of one-dimensional isentropic flow formulations and a direct assessment of the assumptions made in the preceding chapter.

This simplification, however, comes at a cost—primarily by neglecting the detailed geometry of the reactor and potential non-isentropic effects. Therefore, a dedicated section will briefly address flow behavior in micro-channels, particularly the problem of slip at the boundaries. This lays the groundwork for a refined approach in which the reactor is treated as a separate reservoir with its own stagnation conditions.

Recognizing that variations in stagnation conditions inherently correspond to non-isentropic flow behavior, this framework attempts to capture such effects while still applying isentropic analysis to isolated components of the system. This also enables the inclusion of mass flow through leaks in the reactor, whose influence on the Mach number at the inlet throat will be investigated.

Finally, it will be argued why the presented formulations are insufficient to accurately resolve the velocity distribution at the outlet. As a result, possible numerical approaches for addressing this limitation will be discussed.

3.1 Geometry and flow characteristics of the components

The flow geometry can be divided into three simplified sections: gas flows from a reservoir, enters the micro-reactor through an inlet, and exits through an outlet into a vacuum. This model is a deliberate simplification and will serve as the primary representation of the flow path throughout much of this thesis. The only aspect neglected in this simplification is the presence of leaks, which predominantly affect the reactor section, as it is the only part not maintained at a constant pressure by external means.

Reservoir

The reservoir is maintained at constant pressure P_0 and temperature T_0, from which the density ρ_0 can be determined. These values define the stagnation (or total) conditions of the system, where the flow velocity is zero. Throughout this work, regions where stagnation conditions are assumed will be visually distinguished using a gray hue in the figures.

For simplicity, the reservoir is assumed to contain a single gas, characterized by its specific heat ratio γ and molar mass M_m. The analytical formulations employed in this thesis generally express changes in pressure, temperature, and density as ratios relative to the stagnation conditions, making it unnecessary to specify their absolute values when analyzing state changes. However, when calculating quantities such as mass flow rates and dimensionless numbers—including the Reynolds and Knudsen numbers—explicit reference values for stagnation pressure and temperature are required to ensure

proper scaling and physical interpretability. For this purpose, the following gas properties are defined:

$$\gamma = 1.47 \, , \qquad M_m = 28.013 \, \frac{\text{g}}{\text{mol}}$$

representing nitrogen gas (N_2), as it closely approximates the behavior of the gases intended for experimental use.

To enable consistent comparison between the different formulations presented in the following sections, a set of reference stagnation conditions is introduced. Specifically, two stagnation temperatures are defined:

$$T_{0_{min}} = 300 \, \text{K} \quad and \quad T_{0_{min}} = 600 \, \text{K}.$$

These values span the expected operating range, with the former near ambient room temperature and the latter reflecting the maximum temperature the reservoir will be heated to. Both are paired with a reference stagnation pressure of:

$$p_{0_{ref}} = 1.5 \, \text{bar}$$

Which is assumed to yield values near ambient pressure inside the reactor volume.

Inlet and Outlet Nozzles

Inlet The duct connecting the inlet reservoir to the reactor is slightly converging, primarily due to manufacturing constraints. As a result, it acts as a nozzle, accelerating the gas as it expands into the reactor.

Outlet Although the outlet shares the same geometry as the inlet, the gas flows in the opposite direction. One might initially expect it to behave as a subsonic nozzle, since without a converging section upstream, sonic velocities would not typically be achievable. In such a case, the flow would remain subsonic, as choking would not occur. However, under certain conditions, the flow can establish an effective converging section on its own. This allows the flow to become sonic at the entrance of the outlet and to further accelerate into the supersonic regime, effectively forming a supersonic nozzle. [12]
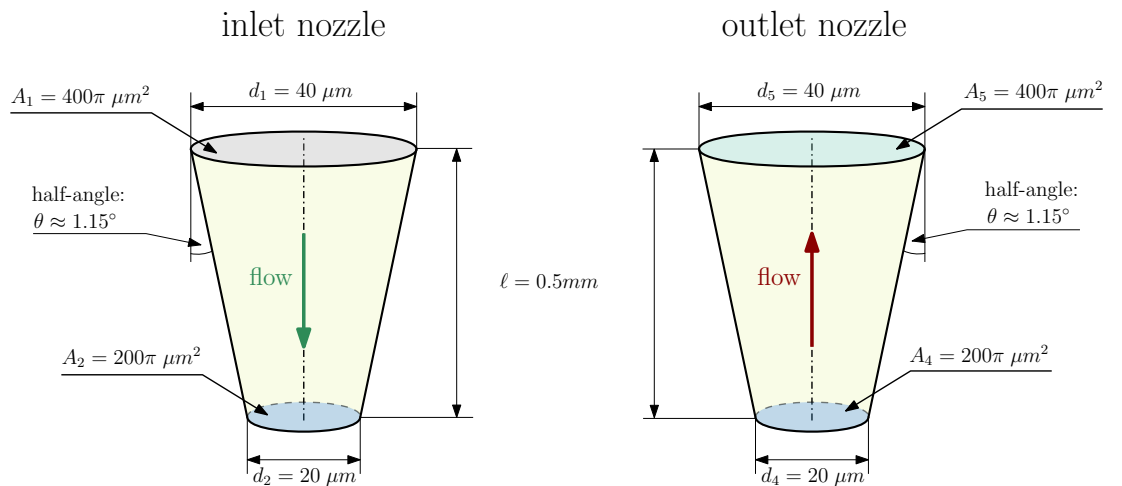
Figure 7. Schematic of the inlet and outlet nozzle assembly: Yellow-shaded regions denote domains where one-dimensional flow is assumed. Flow directions are indicated by colored arrows: green arrows represent subsonic flow and red arrows indicate supersonic flow. In the downstream expansion region, the flow is modeled as two-dimensionally rotationally symmetric (green-shaded). This schematic is not drawn to scale.

Nozzle Flow – Quasi One-Dimensional Approximation   In both nozzle sections, the two-dimensional flow is simplified using the quasi one-dimensional flow model. This approach reduces the local velocity distribution across the duct cross-section to its mean value. Consequently, the velocity field $V(r)$ at each cross-section is approximated by a scalar velocity V. This simplification is valid for ducts with reasonably small variations in cross-sectional area and within the limits of continuum flow, as discussed in Chapter 2.5. One-dimensional flow regions are indicated using a yellow hue, as shown in the nozzle volumes in Figure 7. [4]

Micro-Reactor Volume

The reactor consists of a small, broad cylindrical volume with an opening at the bottom. The sample is pressed onto this opening, resulting in leakage along the interface.
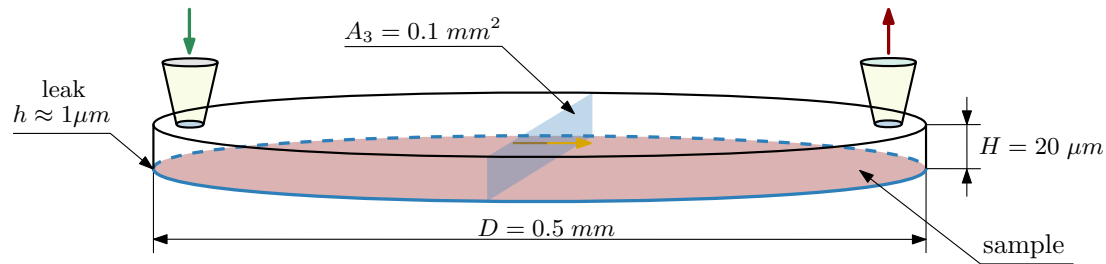
Figure 8. Schematic of the reactor geometry: The reactor volume is shown in blue, representing the region where three-dimensional flow occurs. The sample surface is indicated in red, and the leak is marked by a blue outline along the reactor perimeter. Flow characteristics are depicted by colored arrows: yellow arrows for slow-moving flow, green arrows for subsonic flow, and red arrows for supersonic flow. This diagram is not drawn to scale.

Flow through the Reactor – Three-Dimensional   After the gas exits the inlet nozzle and enters the reactor chamber, the geometry no longer exhibits any symmetry that would allow for a reduction in dimensionality of the velocity field. Additionally, the flow undergoes rapid expansion as the confinement provided by the nozzle walls vanishes and the gas flows past a sharp corner. As a result, the flow field depends on all spatial dimensions. An accurate description of the flow would therefore require solving the full Navier-Stokes equations.

However, this is not feasible using analytical methods alone. To address this, two simplifications will be employed in the following sections. First, the flow through the reactor will be approximated as pseudo one-dimensional, even though this assumption is clearly invalid due to the rapid expansion and the non-isentropic nature of the flow. To overcome these limitations while retaining analytical tractability, Chapter 3.5 will introduce an alternative approach in which the reactor is treated as a separate reservoir with defined stagnation conditions.

Three-dimensional flow regions will be indicated using a blue hue, as shown in the reactor volume in Figure 8.

Vacuum

After exiting the outlet, the gas first expands into a small cylindrical section before freely expanding into the surrounding vacuum. The exact residual pressure in the vacuum chamber does not influence the gas flow inside the assembly. This is because the large pressure ratio between the reactor and the vacuum causes the flow to become choked, meaning that the gas reaches sonic velocity at the nozzle throat. When the flow is choked, the mass flow rate is fixed by the upstream conditions (pressure and

temperature), so further reductions in the downstream (back) pressure have no effect on the flow rate. Due to the sharp pressure drop and the high velocity of the gas particles, the flow transitions to the molecular regime after leaving the outlet nozzle.

Free Jet into Vacuum – Two-Dimensional Similar to the flow expansion into the reactor, the flow exiting into the vacuum chamber cannot be approximated using quasi one-dimensional flow. However, unlike the reactor region, the outlet nozzle possesses radial symmetry, and no further geometry constrains the flow after it exits. Therefore, it is reasonable to assume that the flow inherits this radial symmetry, reducing the spatial parameters of the flow field to the distance from the nozzle and the radial distance from the axis of symmetry, denoted by r.

Furthermore, as the gas expands into the vacuum and the pressure rapidly decreases, the flow undergoes rarefaction. Beyond a certain distance from the nozzle, the continuum assumption breaks down and molecular effects dominate. This transition and possible approaches to describe the flow behavior will be discussed in more detail in Chapter 3.6, where numerical techniques for modeling the plume will be introduced. [4]

## 3.2 Expected flow regimes

Continuum Regime

The whole theory relies heavily on the continuum model. For every location of the flow, but the vacuum, it will be assumed that it suffices to approximate the state variables (T, p,) at certain locations using a simple one-dimensional continuum model presented in more detail in Section 3.3 and use these state variables to calculate the Knudsen number.

The plot in Figure 9 was created by calculating local temperatures and pressures using Equations (2.7) and (2.8) for the reference total conditions given in Section 3.1. Further, calculating Knudsen number using Equation (2.3), where dynamic viscosity is expressed using Sutherland's formula (2.4) with the following empirical constants which are generally used for nitrogen gas [13]:

$$\text{Nitrogen } (N_2): \qquad S_\mu = 111 \text{ K} \qquad T_{ref} = 300.55 \text{ K} \qquad \mu_{ref} = 17.81 \text{ sPa}$$

Now the corresponding Reynolds numbers are calculated using the known relation between dimensionless numbers as stated in Equation (2.12). The values are plotted for two different characteristic lengths, $L_c = 20\ \mu m$ corresponding to throats of the inlet and outlet nozzles and $L_c = 40\ \mu m$ corresponding to the reactor volume and the maximum diameters of the inlet and outlet nozzles.

Figure 9 clearly shows that for a flow with Mach numbers under 3.5 which is expected within the assembly, Knudsen numbers typically remain below 0.1, validating the continuum assumption. Although some regions may fall within the slip regime – where slip boundary conditions have to be introduced to yield more accurate solutions – continuum-based models remain applicable. At the same time, the Reynolds number remains well under 2000, indicating laminar flow, which points to minimal mixing inside the assembly [14, 15].
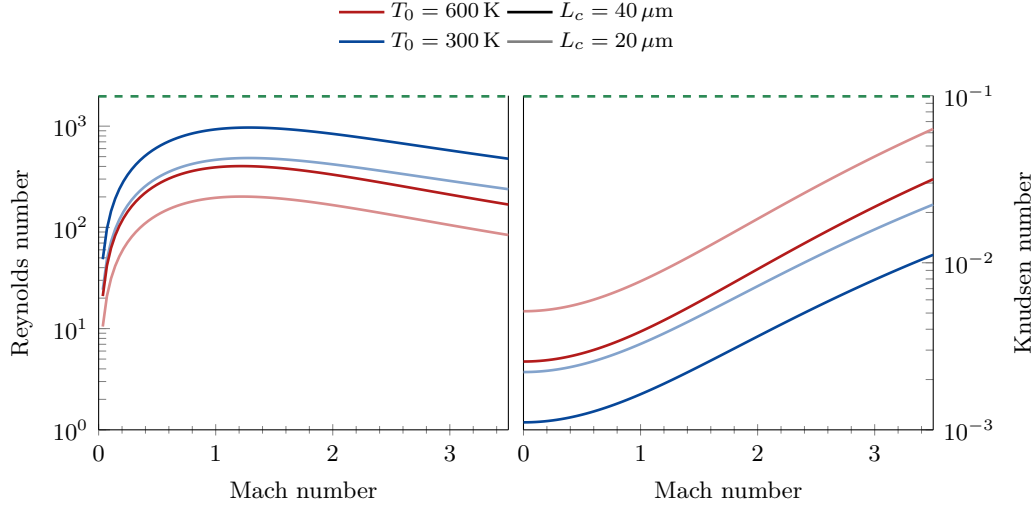
Figure 9. Reynolds and Knudsen numbers as functions of Mach number on logarithmic scales: The plot shows values of Re and Kn for two temperatures ($T_0 = 300\,$K and $T_0 = 600\,$K) and two characteristic lengths ($L_c = 20\,\mu$m and $L_c = 40\,\mu$m) over the expected Mach numbers inside the assembly for Nitrogen. The reference pressure p_{ref} is fixed and chosen such that it corresponds to the limiting cases of the considered T_0 and L_c. The horizontal dotted green line indicates the threshold (Kn = 0.1, Re = 2000) beyond which transitional flow behavior is expected.

Transition to Free Molecular Flow.   Upon exiting the nozzle into vacuum, the gas pressure drops rapidly, leading to a potentially large mean free path. Here, the continuum approximation no longer holds, and using a single characteristic length becomes meaningless. Instead, a local Knudsen number is more appropriate:

$$Kn_L = \frac{\lambda}{\phi}\left|\frac{d\phi}{dx}\right|, \qquad (3.1)$$

where ϕ is a flow property (e.g., p, ρ, T, or U). This definition enables identifying where the flow transitions from continuum to free molecular behavior [16, 17, 10]. Since the focus here is on internal assembly flow, we do not account for rarefied effects outside the nozzle and omit slip-layer modeling for simplicity.

Steady Flow

The assumption of steady flow is justified by the boundary conditions of the system. The reservoir pressure p_0 and temperature T_0 are held constant during operation. Thus, the flow is driven solely by the pressure differential between the reservoir and the vacuum.

Once the initial unsteady effects have decayed, the system reaches an equilibrium state in which the flow remains steady over time. This assumption is valid both within the assembly and in the downstream expansion into the vacuum. [10]

3.3 One-dimensional isentropic variable area flow

By assuming fully isentropic and pseudo one-dimensional flow throughout the assembly, it is possible to determine the state variables at any point, provided that the stagnation conditions and the area ratio between the cross-sectional area at the point of interest A_i and the throat area A^* are known.

However, it must be emphasized that this represents a considerable simplification, as pseudo one-dimensional flow strictly requires the geometry to be approximated by smoothly varying ducts. This assumption neglects the abrupt directional changes that occur as the gas enters and exits the reactor. Moreover, pseudo one-dimensional formulations typically demand gradual changes in cross-sectional area, which clearly is not the case at the sharp transitions near the reactor inlet and outlet. [4]
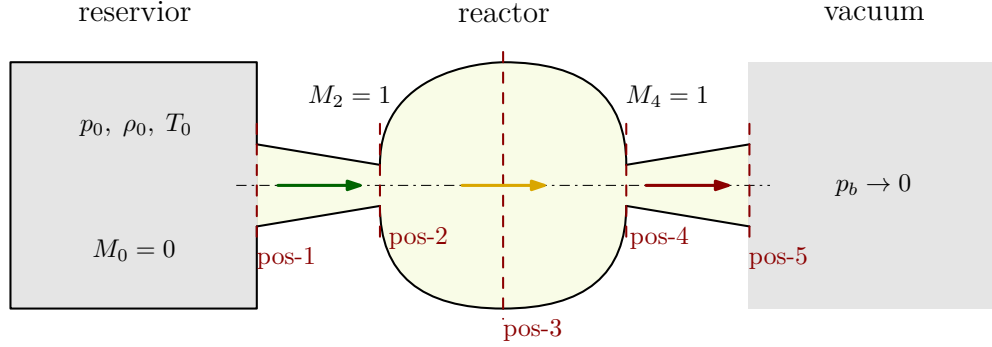
Figure 10. Idealized geometry of the reactor assembly modeled as a one-dimensional variable-area duct. The yellow region represents the domain where quasi one-dimensional isentropic flow is assumed (as described in section 3.1). Grey indicates stagnant gas, the green arrow indicates subsonic flow at the inlet, and the red arrow indicates supersonic flow at the outlet. Flow within the central reactor region is most likely slow-moving.

The simplified geometry can now be recognized as a double-throat configuration, and one-dimensional isentropic flow theory provides two fundamental solutions for this setup. Depending on how steady-state conditions are established, the flow either remains subsonic (with velocity decreasing upon entry into the reactor), or it reaches sonic conditions at the inlet throat and continues to accelerate downstream. Other non-trivial solutions will not be considered. [18, 11]

Calculations

The first step is identifying critical locations where the flow becomes choked. Given the outlet expansion into vacuum, the pressure ratio approaches zero, ensuring choked flow at this location. Because maximum mass-flow through the assembly occurs under choked conditions, the inlet must also be choked to match the mass-flow rate:

$$A_{2,4}, \ p_{2,4}, \ \rho_{2,4}, \ T_{2,4} \quad \xrightarrow{M=1} \quad A^*, \ p^*, \ \rho^*, \ T^*$$

The second critical location corresponds to the stagnation (total) conditions at the inlet nozzle entry, defined by zero velocity:

$$A_1, \ p_1, \ \rho_1, \ T_1 \quad \xrightarrow{M=0} \quad A_0, \ p_0, \ \rho_0, \ T_0$$

Next, cross-sectional areas A_i at all points i defined in chapter 3.1 are used to calculate their respective area ratios relative to the throat area $A_{2,4}$. These area ratios allow for solving equation (2.6), which numerically yields both subsonic and supersonic solutions depending on initial conditions, as detailed in appendix A.2.1.

Subsequently, local state variables relative to stagnation conditions can be computed using equations (2.7)–(2.9). Once stagnation conditions are specified, the local state variables at each location in the assembly are directly determined.

pos-i	$\frac{A_i}{A^*}$	M	$\frac{p_i}{p_t}$	$\frac{\rho_i}{\rho_t}$	$\frac{T_i}{T_t}$	description
1	4	0	1	1	1	reservoir conditions
2	1	1	0.52	0.64	0.81	inlet nozzle exit
3	318.31	~ 0	~ 1	~ 1	~ 1	center of the reactor-volume
		10.55	$3.28 \cdot 10^{-5}$	$8.90 \cdot 10^{-4}$	$3.68 \cdot 10^{-2}$	
4	1	1	0.52	0.64	0.81	outlet nozzle inlet
5	4	0.15	0.98	0.99	0.99	outlet nozzle exit $\neq$ vacuum conditions
		3.06	0.03	0.08	0.31	

Table 1. Isentropic flow properties at various locations along the flow path, assuming fully one-dimensional isentropic conditions throughout the system: Pos-i describes the locations shown in Figure 10. Both values are mathematically valid; green highlights the more physically likely solution, whereas red denotes the less likely one, described in more detail in the interpretation paragraph [calculations: appendix A.1].

With approximate state variables known throughout the assembly, assumptions regarding Reynolds and Knudsen numbers made in chapter 3.2 can now be tested. Given that mass flow is conserved, it can be calculated from equation (2.11) using stagnation conditions and any given pair of cross-sectional area and Mach number at a location i:

$$p_{0_{ref}} = 1.5 \text{ bar} \qquad T_{0_{min}} = 300 \text{ K} \qquad \text{yields} \qquad \dot{m}_1 \approx 1.1 \cdot 10^{-7} \frac{\text{kg}}{\text{s}}$$

$$p_{0_{ref}} = 1.5 \text{ bar} \qquad T_{0_{max}} = 600 \text{ K} \qquad \text{yields} \qquad \dot{m}_2 \approx 7.8 \cdot 10^{-8} \frac{\text{kg}}{\text{s}}$$

The following table summarizes the calculated Reynolds and Knudsen numbers at various points within the assembly for two stagnation temperatures ($T_{0_{min}} = 300$K and $T_{0_{max}} = 600$K) and a stagnation pressure of $p_{0_{ref}} = 1.5$ bar.

$p_0 = 1.5$ bar	T_0	1	2	3 (sub)	3 (sup)	4	5 (sub)	5 (sup)
Re	300 K	0	576	1	6078	576	84	1766
	600 K	0	249	0.4	2928	249	36	764
Kn	300 K	0.001	0.002	0.001	0.2	0.002	0.001	0.009
	600 K	0.003	0.004	0.003	0.5	0.004	0.003	0.02

Table 2. Knudsen and Reynolds numbers for $p_{0_{ref}} = 1.5$ bar, $T_{0_{min}} = 300$ K and $T_{0_{max}} = 500$ K using values from Table 1: The cell highlighted red indicates a transitional regime, whereas the titles colored red and green correspond to the less and more likely solutions from Table 1 respectively. [calculations: Appendix A.1]

Interpretation

The equation relating the area ratio to Mach number typically yields two mathematically consistent solutions at every location (excluding reference points with fixed conditions). These correspond to subsonic and supersonic flows, respectively, and their applicability depends on physical constraints.

For the outlet nozzle, the correct physical solution is supersonic, since the flow exhausts into a vacuum. This holds even in the absence of a clearly defined converging section downstream of the reactor. As discussed in Section 3.2, the flow itself may effectively create a converging geometry as it passes over a sudden geometric contraction, enabling acceleration to sonic conditions and beyond.

While the above analysis establishes a baseline using one-dimensional isentropic flow theory, real micro-channels often exhibit additional phenomena such as slip effects at the boundaries and significant viscous losses. These effects are particularly important at small scales and can substantially alter the actual flow behavior. The next section therefore investigates these microchannel-specific effects and their implications for the validity of the assumptions made thus far.

3.4 Flow behaviors in micro-channels

Going from macroscale channels to microscales introduces significant changes in the behavior of gas flows. A primary factor causing these differences is the phenomenon of velocity slip at surfaces. At small characteristic length scales, the Knudsen number (Kn)—which characterizes the ratio of molecular mean free path to the characteristic dimension of the flow—becomes relatively high ($Kn > 0.001$), placing the flow in the compressible regime with slip boundary conditions.

Most microscale flow behaviors require detailed studies through complex simulations or experiments, as the underlying mechanisms are often not fully explained analytically. This section, therefore, does not provide definitive formulations but instead aims to summarize and reference critical phenomena relevant to microfluidics, primarily drawing from the comprehensive review by Amit Agrawal [19].

Phenomenon of Slip

In contrast to the classical no-slip condition, the slip boundary condition assumes a non-zero tangential velocity of gas molecules at the wall. Maxwell proposed a theoretical model for slip by considering a hypothetical control surface s located half a mean free path from the wall. At this surface, half the gas molecules originate from one mean free path away with a tangential velocity u_λ, while the other half reflect from the wall surface. A fraction σ of the reflected molecules undergo diffuse reflection (taking on the wall velocity u_w), whereas the remaining fraction $(1 - \sigma)$ is reflected specularly (retaining their incoming velocity u_λ).

Expanding u_λ as a second-order Taylor series yields the second-order slip boundary condition commonly employed in continuum analyses:

$$u_g - u_w = \left[\frac{2-\sigma}{\sigma} Kn \left(\frac{\partial u}{\partial n} \right)_s + \frac{Kn^2}{2} \left(\frac{\partial^2 u}{\partial n^2} \right)_s \right] \tag{3.2}$$

Here, u denotes the streamwise velocity, and subscripts g, w, and s indicate gas, wall, and control surface, respectively, while n represents the direction normal to the surface. Crucially, σ denotes the tangential momentum accommodation coefficient (TMAC).

Determining the TMAC accurately for a specific application is critical, as it directly impacts velocity slip at the gas-wall interface, thus significantly influencing rarefied flow

behavior. Typically, TMAC values are obtained experimentally or from computational methods such as direct simulation Monte Carlo (DSMC), as discussed further in the next section.

Additionally, near-wall flow at high Knudsen numbers leads to the formation of a thin region called the Knudsen layer, extending approximately one mean free path from the wall. Within this layer, non-equilibrium effects dominate, and continuum assumptions—including traditional slip conditions—become increasingly inaccurate. Consequently, explicit modeling of the Knudsen layer is necessary for highly rarefied conditions, typically by introducing modified boundary conditions or employing higher-order molecular models.

Sudden Expansion or Contraction

When flow exits from a confined duct into the reactor, the geometry abruptly transitions, resembling a sudden expansion or contraction. As shown by Agrawal [19], under these conditions, the assumption of strict isentropic behavior is no longer valid. The rapid geometric changes induce phenomena such as flow separation, formation of vena contracta regions, and associated pressure and momentum losses.

These non-isentropic effects result in local changes to the stagnation conditions downstream of the geometric discontinuities, meaning static pressure and temperature become influenced by the complex expansion dynamics rather than solely by inlet conditions. Treating the reactor as a reservoir with distinct stagnation conditions allows the analytical framework to accommodate these additional effects. Within this approach, mass flow through the reactor becomes influenced by both geometric configuration and the additional losses due to sudden expansions or contractions.

Surface Roughness

Surface roughness significantly influences effective slip conditions at microscale channel walls, as detailed by Agrawal [19]. At small scales, even slight surface imperfections enhance momentum exchange between gas molecules and the channel wall. This increased interaction effectively reduces the slip length relative to idealized smooth surfaces predicted by Maxwell's model.

Enhanced wall friction due to roughness impacts the pressure distribution and alters local stagnation conditions within the flow. Within the reactor-reservoir modeling approach, surface roughness must therefore be considered through appropriate modifications to boundary conditions, typically by adjusting the TMAC or employing higher-order slip corrections. Including such roughness effects enables more realistic predictions of flow behavior, particularly in regions with significant deviations from classical isentropic relationships. [19, 20]

3.5 Including non-isentropic behaviors

In Section 3.3, the flow within the reactor is modeled under the assumption of being fully isentropic and one-dimensional. This approach simplifies the reactor geometry to that of a variable area duct, resulting in a gradual change of state variables along the flow path from inlet to outlet. However, this formulation does not accurately capture the real geometry of the reactor, particularly the presence of a leak located at the perimeter. Since this location is not explicitly represented in the one-dimensional model, its influence on the flow cannot be accounted for without further simplifications.

Section 3.4 introduces several phenomena relevant to micro-scale flows that are difficult to incorporate analytically. To enable an analytical treatment of the leak and its effects, this section proposes an alternative system formulation. Here, both the inlet

reservoir and the reactor chamber are modeled as separate reservoirs, each defined by their respective stagnation conditions. This simplification decouples the system into two independent problems: one describing the gas expansion from a reservoir into a discharge region, and the other relating to the reactor outlet. This approach effectively models the change in stagnation conditions across the reactor as the result of non-isentropic processes, such as those occurring when the gas enters and exits the reactor.

To reconnect the two reservoirs analytically—initially without including the leak—additional assumptions are made. Stagnation conditions for the reactor are prescribed so that the resulting mass flow at the outlet can be balanced by the inlet conditions, without imposing sonic flow at the inlet throat. To solve this system, a connection between the inlet reservoir conditions and those within the reactor must be established. Two approaches are considered: First, the back pressure and temperature of the discharge region are assumed to correspond to the reactor chamber conditions and are linked isentropically to the inlet reservoir. Second, the temperature is assumed constant, while the pressure follows the same isentropic relation. This simplification effectively models possible heat exchange within the reactor.

Finally, the influence of an additional mass flow rate $\dot{m}_L$ leaving the reactor through the leak is considered. The impact of this additional flow on the inlet Mach number M_{in} is analyzed, aiming to identify an upper limit for the leak mass flow. This limit is defined by the point at which the inlet is again forced to reach sonic conditions. Notably, this analysis does not attempt to derive an explicit formula for $\dot{m}_L$ but instead focuses on the qualitative influence of the leak on the inlet flow conditions.

Formulations without including the leak

In the absence of a leak, the system reduces to a single flow path from the inlet reservoir, through the reactor volume, and out to the vacuum. All mass entering the reactor must exit via the outlet nozzle, eliminating any additional flow paths. Consequently, the boundary conditions become simpler, and standard relationships between the inlet and reactor stagnation states can be applied directly. This section formulates those relationships and illustrates how isentropic or isothermal assumptions may be used without the complexities introduced by a leak.
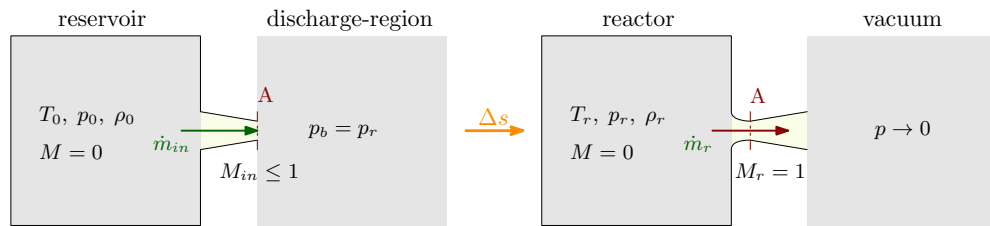
Figure 11. Idealized system separating the reactor from the inlet and outlet regions to account for non-isentropic effects: The yellow regions represent domains where one-dimensional flow is assumed. Grey indicates stagnant gas, green arrow indicates subsonic flow, and the red arrow indicates supersonic flow at the outlet. An entropy change Δs occurs between the gas flowing into the discharge region and the reactor, and the converging section at the outlet represents the flow constraining itself as it accelerates as mentioned in 3.1.

Since this still constitutes a closed system, mass flow must be conserved, thus:

$$\dot{m}_{in} = \dot{m}_r = const.$$

The reactor still discharges into vacuum, this therefore must lead to chocked flow:

$$M_r = 1$$

From the geometry in section 3.1 it is given that:

$$A_{in} = A_r = A$$

The mass flow rates from the reactor into vacuum, can be calculated using the isentropic mass flow equation (2.11)

Reservoir → Reactor

$$\dot{m}_{in} = A\, p_0 \sqrt{\frac{\gamma}{RT}}\, M_{in} \left(1 + \frac{\gamma - 1}{2} M_{in}^2\right)^{-\frac{\gamma+1}{2(\gamma-1)}} \tag{3.3}$$

Reactor → Vacuum

$$\dot{m}_r = A\, p_r \sqrt{\frac{\gamma}{RT}} \left(1 + \frac{\gamma - 1}{2}\right)^{-\frac{\gamma+1}{2(\gamma-1)}} \tag{3.4}$$

Thus from ($\dot{m}_r = \dot{m}_{in} = const.$)

$$A\, p_r \sqrt{\frac{\gamma}{RT}} \left(1 + \frac{\gamma - 1}{2}\right)^{-\frac{\gamma+1}{2(\gamma-1)}} = A\, p_0 \sqrt{\frac{\gamma}{RT}}\, M_{in} \left(1 + \frac{\gamma - 1}{2} M_{in}^2\right)^{-\frac{\gamma+1}{2(\gamma-1)}}$$

Which constitutes the general conservation of mass equation for the system without connecting the state variables of the reservoirs in any way. This will be the starting point for both of the following approaches.

Isentropic approach   In this approach, the reactor is treated as a downstream reservoir with distinct stagnation conditions, implying that irreversibilities have occurred somewhere in the flow path. Instead of modeling the associated entropy generation, local isentropic relations are used to connect the inlet reservoir's stagnation state to the reactor boundary. This method effectively embeds any non-isentropic effects into a "shift" in stagnation values, so the reactor's reduced pressure and/or temperature serve as an isentropic back condition. As a result, flow properties in the nozzles or ducts can still be obtained from standard one-dimensional isentropic equations, even though the actual flow inside the reactor may be more complex.

$$T_b = T_r \quad \rightarrow \quad T_0 = T_r \left(1 + \frac{\gamma - 1}{2} M_{in}^2\right)$$

and

$$p_b = p_r \quad \rightarrow \quad p_0 = p_r \left(1 + \frac{\gamma - 1}{2} M_{in}^2\right)^{\frac{\gamma}{\gamma-1}}$$

Assuming the conditions of the discharge region to match the values in the reactor and using the isentropic relations to express T_0 and p_0 in terms of T_b and P_b the previously defined conservation of mass equation yields:

$$A\, p_r \sqrt{\frac{\gamma}{RT_r}} \left(1 + \frac{\gamma - 1}{2}\right)^{-\frac{\gamma+1}{2(\gamma-1)}}$$

$$=$$

$$A\, p_r \left(1 + \frac{\gamma - 1}{2} M_{in}^2\right)^{\frac{\gamma}{\gamma-1}} \sqrt{\frac{\gamma}{RT_r}} \left(1 + \frac{\gamma - 1}{2} M_{in}\right)^{-\frac{1}{2}} M_{in} \left(1 + \frac{\gamma - 1}{2} M_{in}^2\right)^{-\frac{\gamma+1}{2(\gamma-1)}}$$

Canceling out variables present on both sides and combining the potential expressions on the right side it results a function of M_{in} only dependent on γ, since the summing the exponents equals zero.

$$M_{in} = \left(1 + \frac{\gamma - 1}{2}\right)^{-\frac{\gamma+1}{2(\gamma-1)}} = 0.57 \quad \text{for} \quad \gamma = 1.47$$

Thus resulting in following ratios between the conditions in the reactor and the reservoir and a corresponding mass flow.

$$\frac{T_b}{T_0} = \frac{T_r}{T_0} = 0.93 \ , \quad \frac{p_b}{p_0} = \frac{p_r}{p_0} = 0.79 \ , \quad \frac{\rho_b}{\rho_0} = \frac{\rho_r}{\rho_0} = 0.85 \quad \rightarrow \quad \dot{m} = 6.4 \cdot 10^{-8} \ \frac{\text{kg}}{\text{s}}$$

At reservoir conditions of $T_{0_{max}} = 600$ K and $p_{0_{ref}} = 1.5$ bar.

Constant temperature approach The isothermal approach similarly separates the reactor as an independent reservoir, but enforces a uniform temperature shared with the inlet reservoir. Despite holding temperature constant, a pressure difference can still arise, which inherently indicates a net entropy change. This scenario is plausible if the reactor walls maintain a uniform thermal environment, allowing the gas to remain at the same temperature while the pressure drops. The resulting non-isentropic behavior is thus represented by a constant-temperature condition, and simpler local flow equations remain usable, provided the irreversibilities are captured in the overall pressure imbalance between inlet and reactor.

$$T_r = T_0 = T \neq T_b$$

This approach is going contrary to isentropic formulation, but still seems somehow plausible due to the fact that the gas in the reservoir just like the whole assembly will be preheated to a certain temperature. Since for small cavities the surface area of its walls is much larger in proportion to its internal volume, heat transfer from the walls will be significant even without high mixing due to low Reynolds numbers present in microfluidics.

$$p_r \left(\frac{2}{\gamma+1}\right)^{\frac{\gamma+1}{2(\gamma-1)}} = p_0 \, M_{in} \left(1 + \frac{\gamma-1}{2} M_{in}^2\right)^{-\frac{\gamma+1}{2(\gamma-1)}}$$

Again using the isentropic relation (2.8) for p_0

$$p_r \left(\frac{2}{\gamma+1}\right)^{\frac{\gamma+1}{2(\gamma-1)}} = p_r \left(1 + \frac{\gamma-1}{2} M_{in}^2\right)^{\frac{\gamma}{\gamma-1}} M_{in} \left(1 + \frac{\gamma-1}{2} M^2\right)^{-\frac{\gamma+1}{2(\gamma-1)}}$$

Rearranging leads to an equation only dependent on γ and the mach number Ma_0 at the inlet.

$$\left(\frac{2}{\gamma+1}\right)^{\frac{\gamma+1}{2(\gamma-1)}} = M_{in} \left(1 + \frac{\gamma-1}{2} M_{in}^2\right)^{\frac{1}{2}}$$

Which can be solved analytically, since by squaring both sides and rearranging it resembles a simple quadratic equation:

$$M_{in}^4 + \frac{2}{\gamma-1} M_{in}^2 - \frac{2}{\gamma-1} \left(\frac{2}{\gamma+1}\right)^{\frac{\gamma+1}{\gamma-1}} = 0 \tag{3.5}$$

Now substituting $M_{in}^2 = f \quad \rightarrow \quad M_{in} = \sqrt{f}$

$$f = -\frac{1}{\gamma-1} \pm \sqrt{\frac{1}{(\gamma-1)^2} + \frac{2}{\gamma-1} \left(\frac{2}{\gamma+1}\right)^{\frac{\gamma+1}{\gamma-1}}} \tag{3.6}$$

There is only one real solution for this equation using the positive square root. For $\gamma = 1.47$ we get the solution:

$$f = 0.31 \quad \rightarrow \quad M_{in} = 0.55$$

Which corresponds to the following ration between the conditions in the reactor and the reservoir, which results in the following mass-flow:

$$\frac{T_r}{T_0} \neq \frac{T_b}{T_0} = 0.93 \; , \quad \frac{p_r}{p_0} = 0.79 \; , \quad \frac{\rho_r}{\rho_0} \neq \frac{\rho_b}{\rho_0} = 0.85 \quad \rightarrow \quad \dot{m} = 6.3 \cdot 10^{-8} \, \frac{\mathrm{kg}}{\mathrm{s}}$$

at reservoir conditions of $T_{0_{max}} = 600$ K and $p_{0_{ref}} = 1.5$ bar. Which is in the same order of magnitude as the mass-flow for the fully isentropic formulation in Section 3.3. The discrepancy in mass-flow can be attributed to the change in entropy, indicated by the change in stagnation conditions. Also, now that the temperature of the discharge area and the reactor don't match anymore, heat transfer has to be assumed.

Formulations Including the Leak

Including the leak can be accounted for by assuming an additional mass flow leaving the reactor, which the inlet must compensate:

$$\dot{m}_{in} = \dot{m}_r + \dot{m}_L \quad \Rightarrow \quad \dot{m}_L = \dot{m}_{in} - \dot{m}_r \tag{3.7}$$

This requires an increase in the total conditions of the reservoir to maintain constant conditions inside the reactor. As a consequence, the Mach number increases until the critical pressure ratio (2.10) is reached, resulting in sonic flow at the inlet throat.
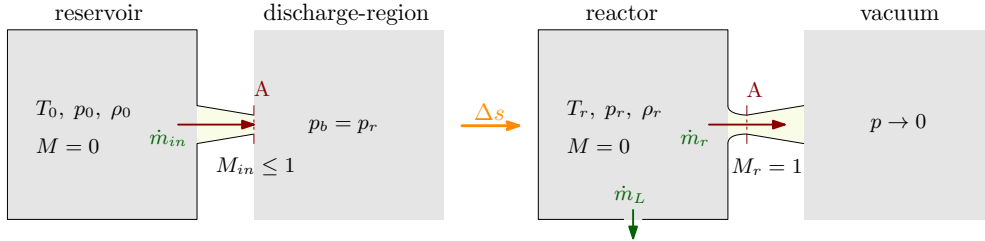
Figure 12. Idealized system separating the reactor from the inlet and outlet regions to account for non-isentropic effects, including a leak path from the reactor: The yellow regions represent domains where one-dimensional flow is assumed, gray indicates stagnant gas, and red arrows indicate supersonic flow. An entropy change Δs occurs between the discharge region and the reactor, while the converging section at the outlet represents the constriction of the flow as it accelerates, as discussed in Section 3.1.

Using the isentropic mass flow Equations (3.3) and (3.4), the effect of the leak can be described by assuming $M_{in} = 1$ and substituting into Equation (3.7). Yielding:

$$\dot{m}_L = A\,p_0\,\sqrt{\frac{\gamma}{RT}}\left(1 + \frac{\gamma-1}{2}\right)^{-\frac{\gamma+1}{2(\gamma-1)}} - A\,p_r\,\sqrt{\frac{\gamma}{RT}}\left(1 + \frac{\gamma-1}{2}\right)^{-\frac{\gamma+1}{2(\gamma-1)}}$$

To relate the reservoir temperature T_0 and pressure p_0 to the reactor conditions, it is again assumed that the conditions in the discharge region and the reactor are identical, thus connecting them through Equations (2.7) and (2.10). This formulation is chosen because it has lead to a higher Mach number at the inlet and therefore reaches sonic conditions sooner. It represents a "worst-case" scenario, as it results in the lowest

additional mass flow required to choke the inlet. After substituting and rearranging the equation yields:

$$\dot{m}_L = A\, p_r \sqrt{\frac{\gamma}{R\, T_r}} \left(1 + \frac{\gamma - 1}{2}\right)^{-\frac{\gamma+1}{2(\gamma-1)}} \tag{3.8}$$

Assuming reservoir conditions of $p_{0_{ref}} = 1.5$ bar and $T_{0_{max}} = 600$ K, the corresponding reservoir state can be calculated using the critical ratios discussed in Section 2.6. The additional mass flow through the leak required to cause sonic conditions at the inlet is then:

$$\dot{m}_L = 3.3 \cdot 10^{-8}\ \frac{\text{kg}}{\text{s}}.$$

This value is approximately half of the mass flow calculated for the disconnected reservoir model. It can thus be concluded that if the mass flow through the leak is comparable to the mass flow through the outlet, this will force the inlet throat to go sonic. This can induce significant changes in the gas behavior downstream of the inlet, such as shock waves and rapid variations in state variables.

Since this setup still constitutes a coupled system—where the leak influences the outlet, for instance, via pressure losses, and vice versa—the exact distribution of the mass flow between the two, as well as the reservoir conditions at which the inlet becomes sonic, must be further investigated through numerical simulation.

3.6 Under-expanded nozzle plume at outlet

Once the gas emerges from the reactor and enters the outlet nozzle, it undergoes a rapid expansion into a low-pressure or near-vacuum environment. This regime differs significantly from the upstream flow: velocity increases dramatically, density drops, and shock waves can appear. The one-dimensional isentropic models used until now cannot fully capture these effects, especially if there is phase change (e.g., condensation) or a transition to free-molecular flow. Hence, more advanced modeling approaches are required. [12, 4]

Method of characteristics

Ideal nozzle design   The method of characteristics is a mathematical technique used to design supersonic nozzles so that gas flows expand smoothly from sonic to supersonic speeds without generating internal shocks. It works by tracing characteristic lines—paths along which flow properties remain constant—through the nozzle region. By aligning the walls with these lines it ensures that each incremental flow turn occurs through a series of controlled expansion waves, rather than abrupt angle changes that could cause shocks. If fully expanded this leads to a straight column of gas leaving the nozzle, where all of its energy is converted into kinetic energy without significant losses due to shocks. This approach is not feasible in this case since the length of the nozzle grows as the back pressure gets lower, the ideal nozzle for the high vacuum found in the surrounding chamber would not be able to fit due to space constraints. [21, 22]

Determining Flow Field for Free Expansion   In supersonic flows, Mach lines form at a specific angle called the Mach angle, given by $\mu = \arcsin\left(\frac{1}{M}\right)$, relative to the flow direction. In three-dimensional flows, these Mach lines form a Mach cone with a half-angle equal to the Mach angle. The method of characteristics is a useful analytical tool for predicting the initial flow properties, including local Mach numbers, densities, velocities, and pressures, immediately after the nozzle exit.

During supersonic expansions, gas flows experience changes in direction described by Prandtl–Meyer expansion fans. These fans set the maximum angle, θ_{max}, that a gas can turn around a sharp corner, defining the outer boundary beyond which gas density and mass flow become very small. The maximum turning angle is calculated by:

$$\theta_{max} = \frac{\pi}{2} \left(\sqrt{\frac{\gamma + 1}{\gamma - 1}} - 1 \right) - \sqrt{\frac{\gamma + 1}{\gamma - 1}} \arctan \sqrt{\frac{\gamma - 1}{\gamma + 1}(M^2 - 1)} + \arctan \sqrt{M^2 - 1} \quad (3.9)$$

Using Equation (3.9) with a Mach number of $M = 3.06$ and $\gamma = 1.47$, the maximum turning angle yields:

$$\theta_{max} = 68.9°$$

This value marks the theoretical limit for gas expansion after leaving the nozzle.

Additionally, under the assumption that the specific heat at constant pressure remains roughly constant, one can view the final jet velocity as arising from the nearly complete conversion of thermal energy into kinetic energy. Because T_0/T in such expansions can be very large, T can often be approximated by the stagnation temperature T_0. The resulting "terminal velocity" v_∞ takes the form

$$v_\infty = \sqrt{2R \cdot \frac{\gamma}{\gamma - 1} \cdot T_0}, \quad (3.10)$$

where γ is the specific heat ratio and R is the specific gas constant. This relation offers a concise way to estimate the maximum jet velocity once the internal energy is nearly fully converted to directed kinetic energy. Using the reference parameters given in Section 3.1 the terminal velocity yields:

$$v_\infty(T_{0min}) = 746 \, \frac{\text{m}}{\text{s}} \qquad \text{and} \qquad v_\infty(T_{0max}) = 1056 \, \frac{\text{m}}{\text{s}}$$

Figure 13 shows the best-matching solution identified in the findings of Cassanova [23], demonstrating how the method of characteristics can predict the post-nozzle flow field under similar conditions.
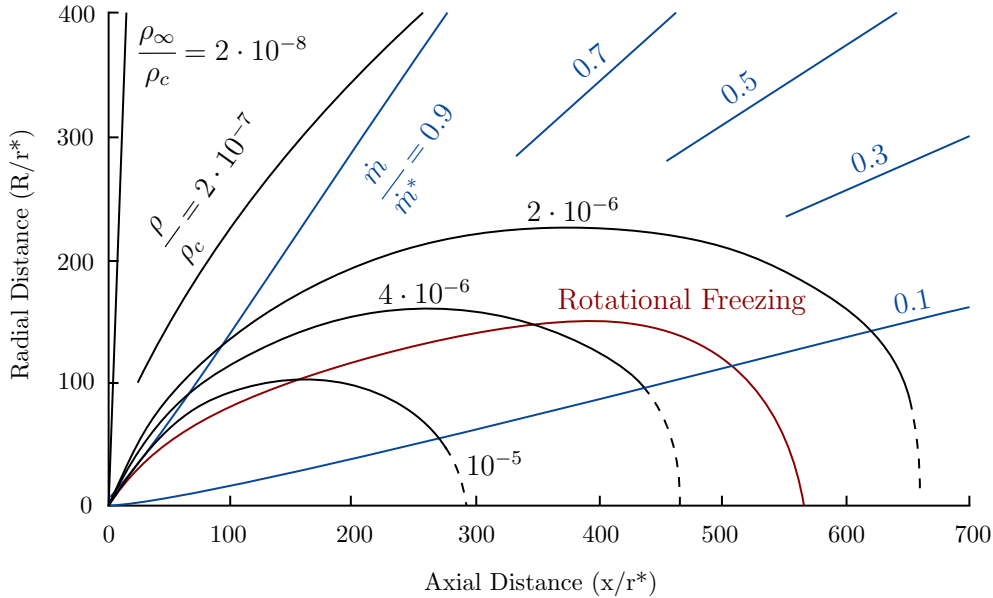
Figure 13. Method of Characteristics Flow Field Solution [23]: for values of $A_0/A^* = 3.73$, $\gamma = 1.4$, $M_e = 2.88$ a half-angle of $\theta = 15°$. The black curves represent isochor lines, the red curve shows rotational freezing for reservoir pressure 1 atm – which corresponds to the pressure in the reactor volume in our case – and the blue curves indicate fractions of the total mass flow enclosed between each curve and the x-axis. This figure has been reduced for readability; see Appendix B for more details.

Rotational freezing occurs in rapidly expanding gases when molecules no longer exchange rotational energy effectively, due to fewer collisions. Typically, rotational energy stops changing after about ten collisions, compared to just one collision for translational energy. When rotational freezing happens, the rotational temperature separates from the translational temperature, affecting the gas's pressure and density profiles significantly. This separation means that predictions near the nozzle exit become less accurate if rotational freezing isn't considered. Rotational freezing happens before translational freezing, meaning rotational energy modes stop adjusting earlier, while translational motion continues to change further downstream.

Boundary layer effects, caused by friction near nozzle walls, also influence gas flow. These effects decrease the exit Mach number and reduce density at the edges of the jet. The boundary layer can create differences between theoretical predictions and experimental results, particularly at lower Knudsen numbers, by redistributing momentum within the gas flow. Adjustments like those provided by the Cohen-Reshotko method help correct predictions by accounting for these boundary layer impacts.

Experiments, such as those by Cassanova and Stephenson, support the method of characteristics for analyzing free expansions and confirm it provides accurate predictions of gas density changes from continuous flow conditions to rarefied conditions. However, these studies also highlight important limitations due to condensation and boundary layer effects. Condensation, especially at pressures between 1–7 atm for nitrogen, significantly alters the gas's thermodynamic properties, limiting the method's accuracy.

In summary, while the method of characteristics effectively predicts initial flow conditions, fully accurate modeling of supersonic expansions must also consider rotational freezing, boundary layer effects, and potential condensation. [12, 24, 25]

Navier-Stokes Equations

A second option is to solve the Navier–Stokes equations numerically, using no-slip or first/second-order slip boundary conditions as appropriate. Near the nozzle exit—where the flow is still predominantly continuum—Navier–Stokes simulations can provide detailed velocity and pressure fields, including shock structures and boundary-layer effects. As the gas expands and its density decreases, however, continuum assumptions start to break down. While slip or transitional models can extend the validity range, ultimately they cannot fully describe the molecular-level interactions that dominate in highly rarefied regions. Consequently, beyond a certain distance from the nozzle exit or under conditions favorable to partial condensation, Navier–Stokes solutions must be supplemented by more advanced kinetic-based methods. [26, 4]

Direct simulation Monte Carlo (DSMC)

To address the shortcomings of both the method of characteristics (under non-ideal conditions) and Navier–Stokes (when rarefaction becomes significant), the Direct Simulation Monte Carlo (DSMC) method is indispensable. DSMC performs a stochastic simulation of molecular motion and collisions, making it particularly well suited for:

- Transitional Regimes: Where the mean free path is comparable to or larger than the nozzle scale, DSMC accurately captures Knudsen-layer effects and velocity-slip phenomena.

- Condensation Phenomena: By including collision physics and intermolecular potentials, DSMC can handle the onset of condensation or two-phase flow more reliably than continuum or purely isentropic approaches. [11]

- Free Expansion: As the jet spreads into the vacuum and transitions toward free-molecular flow, DSMC seamlessly handles extremely high Mach numbers and very low densities, maintaining physical fidelity across a wide range of Knudsen numbers.

Although more computationally expensive than continuum-based methods, DSMC provides the most robust depiction of outlet flows—particularly for condensable gases like nitrogen—and ensures high accuracy from near-nozzle regions all the way to the fully rarefied state. [6, 27]

Summary

Overall, while the method of characteristics remains a cornerstone of ideal nozzle design and near-exit expansions (including the prediction of Prandtl–Meyer fans and maximum turning angles), condensation and severe rarefaction invalidate its purely isentropic assumption further downstream. Navier–Stokes simulations can capture intermediate regimes near the exit, but eventually fail in the highly rarefied or partially condensed flow domain. For a comprehensive treatment of under-expanded plumes—particularly with nitrogen or other condensable working fluids—the DSMC technique offers the necessary level of detail, bridging the gap from continuum flow at the nozzle exit to free-molecular flow far downstream.

Discussion

The analytical work presented in this thesis has provided a basic understanding of gas flow behavior within the micro-reactor assembly. Starting with the detailed geometrical characterization in Section 3.1, we simplified the reactor's complex structure into discrete segments—reservoir, inlet/outlet nozzles, and the central reaction volume—to enable a quasi one-dimensional approximation. This initial abstraction set the stage for applying isentropic flow theory and provided a baseline for the values of characteristic lengths and flow areas.

In Section 3.2, the expected flow regimes were determined by calculating key dimensionless numbers. The analysis revealed that, under typical operating conditions, the system predominantly falls within the continuum regime with slip at the walls. This finding is crucial because it validates the use of continuum-based formulations for the majority of the flow, while also pointing to specific zones (e.g., near the outlet) where the transition to molecular flow might occur.

Section 3.3 delved into one-dimensional isentropic variable area flow, where state variables were linked to changes in cross-sectional areas along the flow path. Although two mathematically viable solutions emerged—corresponding to subsonic and supersonic branches—the physical reasoning, supported by the geometry and boundary conditions, guided the selection of the more likely scenario of subsonic, slow moving flow inside the reactor and supersonic flow leaving the outlet.

The discussion then moved to the microscale in Section 3.4, addressing flow behaviors in micro channels. Here, factors such as slip effects, surface roughness, and sudden geometric expansions were discussed qualitatively. These effects, which become significant as the characteristic lengths shrink, hint at deviations from classical isentropic behavior and suggest that empirical corrections or advanced simulation techniques may be necessary for a more accurate description.

Recognizing these limitations, Section 3.5 extended the analysis to include non-isentropic behaviors. By treating the reservoir and the reactor as distinct entities with independent stagnation conditions, the approach captured the impact of leaks on the overall mass flow and the flow velocity at the inlet. Although this formulation introduces further approximations, it serves to bridge the gap between idealized isentropic models and the more complex reality of the system.

Finally, Section 3.6 addressed the under-expanded nozzle plume at the outlet, where rapid expansion, shock structures, and rarefaction effects dominate. The discussion here emphasized that while traditional one-dimensional models offer a first approximation, advanced methods such as the method of characteristics, Navier–Stokes simulations, or DSMC are required to capture the full complexity of the free expansion into vacuum.

Conclusion

The primary goal of this thesis was to develop an accessible analytical framework to predict gas flow behavior within high-pressure micro-reactor cells, emphasizing continuum gas flows. Through analytical modeling, the study successfully characterized the dominant flow regimes, identified critical state variables, and provided estimations of flow velocities at key reactor points. Although, the initial objectives—quantifying the impact of leakage and determining the velocity distribution after the reactor outlet—were not fully realized, the research established a solid foundational understanding of these factors and their influence on reactor behavior.

The findings demonstrated that isentropic flow assumptions could effectively capture macroscopic gas behavior, especially when considering microscale effects such as slip conditions and non-isentropic phenomena. Nonetheless, further refinement is required, particularly in accurately modeling leak dynamics and the complex transitional behaviors observed at the reactor outlet as the gas expands into vacuum conditions.

Looking forward, detailed numerical simulations, including methods like Direct Simulation Monte Carlo (DSMC), should be pursued to better represent rarefied flow conditions and explicitly quantify leakage effects. Additionally, empirical validation through experimental investigations is essential to refine these analytical models, thereby improving their reliability and extending their applicability.

Symbols and Notation

Primary Symbols and Definitions

A	cross-sectional area	$\dot{m}$	mass flow
P_w	wetted perimeter	p	pressure
ρ	mass density	R	specific gas constant
μ	dynamic viscosity	s	entropy
ν	kinematic viscosity	T	absolute temperature
c_p	specific heat at const. pressure	u	velocity parallel to flow
c_v	specific heat at const. volume	v	velocity perpendicular to flow
γ	ratio of specific heats	V	speed of flow
M_m	molecular mass	V_∞	maximum speed at absolute zero
L_c	characteristic length	σ	TMAC
a	speed of sound	θ	shock-wave angle
M	Mach number	μ	Mach angle, $\sin^{-1}\frac{1}{Ma}$
Re	Reynolds number	ν	Prandtl-Meyer angle
Kn	Knudsen number		

Subscripts

Generally used:

∞	free-stream conditions
$*$	critical conditions typically called the throat ($M = 1$)
0	stagnation/reservoir conditions ($M = 0$)

Used in Section 3.3 as pos-i where $i \in \{1, 2, 3, 4, 5\}$ stands for:

1	inlet nozzle inlet conditions (assumed to equal reservoir conditions)
2	inlet nozzle exit conditions
3	reactor center conditions
4	outlet nozzle inlet conditions
5	outlet nozzle exit conditions

Used in Section 3.5:

r	reactor conditions
in	inlet conditions
b	reservoir discharge region conditions
L	leak conditions

Notations

`[perf]`	thermally and calorically perfect gas.
`[therm perf]`	thermally perfect but calorically imperfect gas.
`[isen]`	isentropic flow process (not valid for shock waves).
`[adiab]`	adiabatic process (no heat transfer, may or may not be isentropic).

Formulas and Equations

This formulary gathers the key equations used in your thesis on micro-reactor gas dynamics. Only the most important, frequently referenced equations are included, with some additional useful relations used to derive some of the given equations.

Thermodynamics

- **Thermal Equation of State:** An equation of state relates pressure, specific volume, and temperature:
$$p = p(v, T)$$

- **Ideal Gas Law (Thermally Perfect):**

$$p = \rho R T \quad \text{[therm perf]}$$

- **1D Euler Equation (for a perfect gas):**

$$\frac{1}{\rho} \, dp + V \, dV = 0 \quad \text{[therm perf]}$$

Navier–Stokes Equations (Compressible, Viscous Flow)

The general form of the Navier–Stokes equations for a compressible, viscous fluid (assuming Newtonian fluid and neglecting external forces other than pressure) is given by:

- **Continuity equation:**
$$\frac{\partial \rho}{\partial t} + \nabla \cdot (\rho \vec{V}) = 0$$

- **Momentum equation:**

$$\frac{\partial (\rho \vec{V})}{\partial t} + \nabla \cdot (\rho \vec{V} \vec{V}) = -\nabla p + \nabla \cdot \boldsymbol{\tau}$$

  where the viscous stress tensor for Newtonian fluids is defined as:

$$\boldsymbol{\tau} = \mu \left[(\nabla \vec{V}) + (\nabla \vec{V})^T - \frac{2}{3} (\nabla \cdot \vec{V}) \boldsymbol{I} \right]$$

  Here, μ is dynamic viscosity, and $\boldsymbol{I}$ is the identity tensor.

- **Energy equation:**

$$\frac{\partial}{\partial t} (\rho e_t) + \nabla \cdot \left[\vec{V} (\rho e_t + p) \right] = \nabla \cdot \left(k \nabla T + \boldsymbol{\tau} \cdot \vec{V} \right)$$

  where total energy per unit mass is defined as:

$$e_t = e + \frac{|\vec{V}|^2}{2}$$

  and k represents the thermal conductivity.

Control Volume Analysis

- **Continuity Equation:**

$$\frac{d}{dt} \int_V \rho \, dV + \int_S \rho \vec{V} \cdot d\vec{A} = 0$$

For steady, one-dimensional flow (constant cross-sectional area):

$$\sum \rho V A = 0$$

Continuous One-Dimensional Flow

- **Speed of Sound:**

$$a = \sqrt{\left(\frac{\partial p}{\partial \rho}\right)_s} = \sqrt{\gamma \frac{p}{\rho}} = \sqrt{\gamma R T} \quad \text{[therm perf]}$$

- **Mach Number:**

$$M = \frac{V}{a} \quad (2.5)$$

- **Area-Mach Relation (Isentropic Flow):**

$$\frac{A}{A^*} = \frac{1}{M}\left[\frac{2}{\gamma+1}\left(1 + \frac{\gamma-1}{2}M^2\right)\right]^{\frac{\gamma+1}{2(\gamma-1)}} \quad \text{[isen, perf]} \quad (2.6)$$

- **Isentropic Relations:** From the constant p/ρ^γ we obtain:

$$\frac{p}{p_0} = \left(\frac{\rho}{\rho_0}\right)^\gamma = \left(\frac{T}{T_0}\right)^{\frac{\gamma}{\gamma-1}} = \left(\frac{a}{a_0}\right)^{\frac{2\gamma}{\gamma-1}} \quad \text{[isen, perf]}$$

- **Bernoulli's Equation for Compressible Flow:**

$$\frac{\gamma}{\gamma-1}\left(\frac{p_0}{\rho_0}\right)^{\frac{\gamma-1}{\gamma}}\left(\frac{p}{p_0}\right)^{\frac{1}{\gamma}} + \frac{V^2}{2} = \frac{\gamma}{\gamma-1}\frac{p_0}{\rho_0} \quad \text{[isen, perf]}$$

- **Stagnation/Total Relations:**

$$\frac{T}{T_0} = \left(1 + \frac{\gamma-1}{2}M^2\right)^{-1} \quad \text{[adiab, perf]} \quad (2.7)$$

$$\frac{p}{p_0} = \left(1 + \frac{\gamma-1}{2}M^2\right)^{-\frac{\gamma}{\gamma-1}} \quad \text{[isen, perf]} \quad (2.8)$$

$$\frac{\rho}{\rho_0} = \left(1 + \frac{\gamma-1}{2}M^2\right)^{-\frac{1}{\gamma-1}} \quad \text{[isen, perf]} \quad (2.9)$$

- **Critical Ratios:**

$$\frac{T_0}{T^*} = \frac{\gamma+1}{2} \qquad \frac{\rho_0}{\rho^*} = \left(\frac{\gamma+1}{2}\right)^{\frac{1}{\gamma-1}} \qquad \frac{p_0}{p^*} = \left(\frac{\gamma+1}{2}\right)^{\frac{\gamma}{\gamma-1}} \quad (2.10)$$

Dimensionless Numbers & Viscosity

- **Reynolds Number:**

$$Re = \frac{\rho \, V \, L}{\mu} = \frac{V \, L}{\nu} \quad (2.2)$$

- **Knudsen Number:**

$$Kn = \frac{\lambda}{L_c} = \quad (2.3)$$

- **Relation between major dimensionless numbers**

$$Kn = \frac{M}{Re} \sqrt{\frac{\gamma \pi}{2}} \quad (2.12)$$

- **Sutherland's Formula (Dynamic Viscosity):**

$$\mu(T) = \mu_0 \left(\frac{T}{T_0} \right)^{3/2} \frac{T_0 + S}{T + S} \quad (2.4)$$

Mass Flow Rate (Compressible, Isentropic Flow)

$$\dot{m} = A \, p_0 \sqrt{\frac{\gamma}{R \, T_0}} \, M \left(1 + \frac{\gamma - 1}{2} M^2 \right)^{-\frac{\gamma + 1}{2(\gamma - 1)}} \quad (2.11)$$

Additional Useful Relations

- **Prandtl-Meyer Function (Expansion Fan):**

$$\nu(M) = \sqrt{\frac{\gamma + 1}{\gamma - 1}} \arctan\left(\sqrt{\frac{\gamma - 1}{\gamma + 1}(M^2 - 1)} \right) - \arctan\left(\sqrt{M^2 - 1} \right)$$

The maximum turning angle is given by:

$$\theta_{\max} = \nu(M \to \infty) - \nu(M) \quad (3.9)$$

List of Figures

List of Tables

References

1. LAGIN, A. *Advancing Single-Atom Catalysis: Development of an Apparatus for Reactions at Near Ambient Pressure* [Poster presented at the Institute of Applied Physics, Vienna University of Technology (TU Wien), Surface Physics Group]. 2025. Project presentation.

2. LEISHMAN, J. Gordon. Internal Flows [online]. 2023 [visited on 2024-07-25]. Available from DOI: `10.15394/eaglepub.2022.1066.n26`. Book Title: Introduction to Aerospace Flight Vehicles Publisher: Embry-Riddle Aeronautical University.

3. ÇENGEL, Yunus A.; CIMBALA, John M. *Fluid Mechanics: Fundamentals and Applications.* 4th. New York, NY: McGraw Hill, LLC, 2017. Mechanical Engineering.

4. ANDERSON, John D. *Modern Compressible Flow: With Historical Perspective.* 4th. New York: McGraw-Hill Education, 2021. ISBN 9781260570556.

5. RAPP, Bastian E. *Microfluidics: Modeling, Mechanics and Mathematics.* Oxford, UK: Elsevier, 2017. ISBN 978-1-4557-3141-1. Available from DOI: `10.1016/C2012-0-02230-2`.

6. PUTIGNANO, Massimiliano. *Supersonic Gas-Jet Based Beam Profile Monitor.* Liverpool, UK, 2012. PhilosophiæDoctor (PhD). University of Liverpool.

7. HALWIDL, Daniel. *Development of an Effusive Molecular Beam Apparatus* [online]. Wiesbaden, 2016 [visited on 2023-09-28]. Available from DOI: `10.1007/978-3-658-13536-2`. PhD thesis. Springer Fachmedien Wiesbaden.

8. CANTWELL, Brian. *AA210A: Fundamentals of Compressible Flow - Course Introduction.* 2020. Presentation slide with a rocket test image on cover.

9. BENSON, Ben. *Mass Flow Rate Equations* [online]. [N.d.]. [visited on 2025-01-27]. Available from: `https://www.grc.nasa.gov/www/k-12/VirtualAero/BottleRocket/airplane/mchkdrv.html`.

10. LI, Wen-Hsiung; LAM, Sau-Hai. *Principles of Fluid Mechanics.* Reading, Massachusetts: Addison-Wesley, 1964. Addison-Wesley Series in Engineering Science: Mechanics and Thermodynamics. Consulting editors: Bernard Budiansky and Howard W. Emmons.

11. *Fundamentals of Gas Dynamics* [online]. Princeton University Press, 1958 [visited on 2025-01-21]. ISBN 9780691626499. Available from: `http://www.jstor.org/stable/j.ctt183pg9x`.

12. JOUSTEN, Karl (ed.). *Handbook of vacuum technology.* Second, completely revised and updated edition. Weinheim: Wiley-VCH Verlag GmbH & Co. KGaA, 2016. ISBN 978-3-527-41338-6 978-3-527-68824-1 978-3-527-68823-4 978-3-527-68826-5 978-3-527-68825-8.

13. KIM, Youn J.; KIM, You-Jae; HAN, J. -G. *Numerical analysis of flow characteristics of an atmospheric plasma torch.* 2004. Available from arXiv: `physics/0410237` `[physics.class-ph]`.

14. AMES RESEARCH STAFF. *Equations, Tables, and Charts for Compressible Flow.* Moffett Field, CA, 1953. Tech. rep., Report 1135. National Advisory Committee for Aeronautics. Available also from: `https://ntrs.nasa.gov/api/citations/19930091059/downloads/19930091059.pdf`.

15. COMSOL. *Microfluidics Module User's Guide.* Stockholm, Sweden: COMSOL AB, 2022. Version: COMSOL 6.1, Part number: CM021901. Available at: `www.comsol.com`.

16. BIRD, G. A. *DSMC - The DSMC method.* Version 1.2. S.l.: G. A. Bird, 2013. ISBN 978-1-4921-1290-7.

17. GRABE, Martin. Numerical Simulation of Nitrogen Nozzle Expansion Using Kinetic and Continuum Approaches. In: *Proceedings of the 59th International Astronautical Conference 2008.* Glasgow, 2008. Open Access. Available at `https://elib.dlr.de/55152/`.

18. SALAS, M.D.; ABARBANEL, S.; GOTTLIEB, D. Multiple steady states for characteristic initial value problems. *Applied Numerical Mathematics.* 1986, vol. 2, no. 3, pp. 193–210. ISSN 0168-9274. Available from DOI: `https://doi.org/10.1016/0168-9274(86)90028-0`. Special Issue in Honor of Milt Rose's Sixtieth Birthday.

19. AGRAWAL, Amit. A Comprehensive Review on Gas Flow in Microchannels. *International Journal of Micro-Nano Scale Transport* [online]. 2011, vol. 2, no. 1, pp. 1–40 [visited on 2024-07-09]. ISSN 1759-3093. Available from: `http://doi.org/10.1260/1759-3093.2.1.1`. Number: 1 Publisher: Multi-Science Publishing.

20. WANG, Moran; LAN, Xudong; LI, Zhixin. Analyses of gas flows in micro- and nanochannels. *International Journal of Heat and Mass Transfer* [online]. 2008, vol. 51, no. 13-14, pp. 3630–3641 [visited on 2024-11-18]. ISSN 00179310. Available from DOI: `10.1016/j.ijheatmasstransfer.2007.10.011`.

21. KHARE, Shivang; SAHA, Ujjwal K. Rocket nozzles: 75 years of research and development. *Sādhanā* [online]. 2021, vol. 46, no. 2, p. 76 [visited on 2024-08-21]. ISSN 0973-7677. Available from DOI: `10.1007/s12046-021-01584-6`.

22. FERNANDES, Tiago; SOUZA, Alain; AFONSO, Frederico. A shape design optimization methodology based on the method of characteristics for rocket nozzles. *CEAS Space Journal* [online]. 2023, vol. 15, no. 6, pp. 867–879 [visited on 2024-08-21]. ISSN 1868-2510. Available from DOI: `10.1007/s12567-023-00511-1`.

23. CASSANOVA, R. A.; STEPHENSON, W. B. *Expansion of a Jet into Near Vacuum.* 1965-08. Tech. rep., AEDC-TR-65-151. Aerospace Environmental Facility, Arnold Engineering Development Center, Air Force Systems Command, Arnold Air Force Station, Tennessee. Available also from: `https://apps.dtic.mil/sti/tr/pdf/AD0469041.pdf`. Approved for public release; distribution is unlimited.

24. ROBERTSON, S. J. *Investigation of the steady expansion of a gaseous axisymmetric jet into a vacuum Final report* [online]. 1970-01. [visited on 2024-08-22]. Tech. rep., HREC-1490-2. Available from: `https://ntrs.nasa.gov/citations/19700021503`. NTRS Author Affiliations: Lockheed Missiles and Space Co. NTRS Document ID: 19700021503 NTRS Research Center: Legacy CDMS (CDMS).

25. *Zucrow, Hoffman - Gas Dynamics, Vol. 2 - 1977.pdf* [online]. [N.d.]. [visited on 2024-08-22]. Available from: `http://ftp.demec.ufpr.br/CFD/bibliografia/Zucrow,%20%20Hoffman%20-%20Gas%20Dynamics,%20Vol.%202%20-%201977.pdf`.

26. ANDERSON, John D. *Fundamentals of aerodynamics.* Sixth edition. New York, NY: McGraw Hill Education, 2017. McGraw-Hill series in aeronautical and aerospace engineering. ISBN 978-1-259-12991-9.

27. LIU, Minghou; ZHANG, Xianfeng; ZHANG, Genxuan; CHEN, Yiliang. Study on micronozzle flow and propulsion performance using DSMC and continuum methods. *Acta Mechanica Sinica* [online]. 2006, vol. 22, no. 5, pp. 409–416 [visited on 2025-02-24]. ISSN 1614-3116. Available from DOI: 10.1007/s10409-006-0020-y.

A Calculations

A.1 Algebraic Calculations

Performed in SMath: https://smath.com/

Variable Definitions:

$$\gamma := 1.47 \qquad M_m := 28.01 \; \frac{gram}{mol} \qquad R_s := \frac{R_m}{M_m} = 296.8394 \cdot \frac{1}{K} \; \frac{J}{kg}$$

$$A_3 := 100000 \; micron^2 = 0.1 \; mm^2 \qquad A_4 := 100 \cdot \pi \; micron^2 \qquad A_5 := 400 \cdot \pi \; micron^2$$

$$T_t := 500 \; K \quad p_t := 1.5 \; bar \qquad A_2 := A_4 \qquad A_1 := A_5$$

$$L_{c.1} := 40 \; micron \qquad L_{c.2} := 40 \; micron \qquad L_{c.3} := 40 \; micron \qquad L_{c.4} := 20 \; micron \qquad L_{c.5} := 40 \; micron$$

Function Definitions:

Isentropic Massflow:

$$massflow\left(\gamma, M, A, T_t, p_t\right) := A \cdot p_t \cdot \sqrt{\frac{\gamma}{R_s \cdot T_t}} \cdot M \cdot \left(1 + \frac{\gamma - 1}{2} \cdot M^2\right)^{-\frac{\gamma+1}{2 \cdot (\gamma-1)}}$$

Dynamic Viscosity using sutherlands formular:

$$\mu_{ref} := 1.716 \cdot 10^{-5} \; \frac{N \; s}{m^2} \qquad T_{ref} := 276 \; K \qquad S_\mu := 111 \; K \qquad p_{crit.ratio} := \left(\frac{2}{\gamma+1}\right)^{\frac{\gamma}{\gamma-1}} = 0.5168$$

$$sutherland\left(T\right) := \mu_{ref} \cdot \left(\frac{T}{T_{ref}}\right)^{\frac{3}{2}} \cdot \frac{T_{ref} + S_\mu}{T + S_\mu} \qquad T_{crit.ratio} := \frac{2}{\gamma+1} = 0.8097$$

Knudsen number:

$$knudsen\left(p, T, L_c\right) := \frac{sutherland\left(T\right) \cdot R_s}{p \cdot L_c} \cdot \sqrt{\frac{\pi \cdot M_m \cdot T}{2 \; k \; N_A}}$$

Reynolds number:

$$reynolds\left(p, T, L_c, Ma, \gamma\right) := \frac{knudsen\left(p, T, L_c\right)}{Ma} \cdot \sqrt{\frac{2}{\gamma \cdot \pi}}$$

Isentropic Relations:

$$temp\_to\_total\left(\gamma, M\right) := \left(1 + \frac{\gamma-1}{2} \cdot M^2\right)^{-1} \qquad pressure\_to\_total\left(\gamma, M\right) := \left(1 + \frac{\gamma-1}{2} \cdot M^2\right)^{-\frac{\gamma}{\gamma-1}}$$

$$density\_to\_total\left(\gamma, M\right) := \left(1 + \frac{\gamma-1}{2} \cdot M^2\right)^{-\frac{1}{\gamma-1}}$$

Machnumber solvers:

$$solve\_machnumber\_sub\left(A_{ratio}, \gamma\right) := solve\left(\frac{1}{M} \cdot \left(\left(\frac{2}{\gamma+1}\right) \cdot \left(1 + \frac{\gamma-1}{2} \cdot M^2\right)\right)^{\frac{\gamma+1}{2 \cdot (\gamma-1)}} - A_{ratio} = 0, M, 0, 1\right)$$

$$solve\_machnumber\_super\left(A_{ratio}, \gamma\right) := solve\left(\frac{1}{M} \cdot \left(\left(\frac{2}{\gamma+1}\right) \cdot \left(1 + \frac{\gamma-1}{2} \cdot M^2\right)\right)^{\frac{\gamma+1}{2 \cdot (\gamma-1)}} - A_{ratio} = 0, M, 1, 12\right)$$

Chapter 3.3: one-dimensional isentropic case

Position 3 (middle of Reactor):

From external Solver:

$$M_{3.1} := solve\_machnumber\_sub\left(318, \gamma\right) = \blacksquare \qquad M_{3.2} := solve\_machnumber\_super\left(318, \gamma\right) = 10.543$$

$$M_{3.1} := 0.0018$$

$$m_{3.1} := massflow\left(\gamma, M_{3.1}, A_3, T_t, p_t\right) = 8.4972 \cdot 10^{-8} \; \frac{kg}{s} \qquad m_{3.2} := massflow\left(\gamma, M_{3.2}, A_3, T_t, p_t\right) = 8.5253 \cdot 10^{-8} \; \frac{kg}{s}$$

$p_{3.1.to.total} := pressure\_to\_total \left(\gamma , M_{3.1} \right) = 1$
$T_{3.1.to.total} := temp\_to\_total \left(\gamma , M_{3.1} \right) = 1$

$p_{3.2.to.total} := pressure\_to\_total \left(\gamma , M_{3.2} \right) = 3.2891 \cdot 10^{-5}$
$T_{3.2.to.total} := temp\_to\_total \left(\gamma , M_{3.2} \right) = 0.0369$

Position 2 & 4 (nozzle throats):

$m_{2.4} := massflow \left(\gamma , 1 , A_4 , T_t , p_t \right) = 8.517 \cdot 10^{-8} \frac{kg}{s}$

$p_{2.4.to.total} := pressure\_to\_total \left(\gamma , 1 \right) = 0.5168$

$\rho_{2.4.to.total} := density\_to\_total \left(\gamma , 1 \right) = 0.6382$

$T_{2.4.to.total} := temp\_to\_total \left(\gamma , 1 \right) = 0.8097$

Position 5 (outlet nozzle exit plane):

$M_{5.1} := solve\_machnumber\_sub \left(4 , \gamma \right) = 0.1455$

$m_{5.1} := massflow \left(\gamma , M_{5.1} , A_5 , T_t , p_t \right) = 8.5169 \cdot 10^{-8} \frac{kg}{s}$

$p_{5.1.to.total} := pressure\_to\_total \left(\gamma , M_{5.1} \right) = 0.9846$

$\rho_{5.1.to.total} := density\_to\_total \left(\gamma , M_{5.1} \right) = 0.9895$

$T_{5.1.to.total} := temp\_to\_total \left(\gamma , M_{5.1} \right) = 0.9951$

$M_{5.2} := solve\_machnumber\_super \left(4 , \gamma \right) = 3.063$

$m_{5.2} := massflow \left(\gamma , M_{5.2} , A_5 , T_t , p_t \right) = 8.517 \cdot 10^{-8} \frac{kg}{s}$

$p_{5.2.to.total} := pressure\_to\_total \left(\gamma , M_{5.2} \right) = 0.0262$

$\rho_{5.2.to.total} := density\_to\_total \left(\gamma , M_{5.2} \right) = 0.0839$

$T_{5.2.to.total} := temp\_to\_total \left(\gamma , M_{5.2} \right) = 0.312$

Chapter 3.3: one-dimensional isentropic knudsen and reynolds numbers

knudsen numbers:

$Kn_1 := knudsen \left(p_t , T_t , L_{c.1} \right) = 0.0021$ $Kn_{2.4} := knudsen \left(p_t \cdot p_{2.4.to.total} , T_t \cdot T_{2.4.to.total} , L_{c.2} \right) = 0.0032$

$Kn_{3.1} := knudsen \left(p_t \cdot p_{3.1.to.total} , T_t \cdot T_{3.1.to.total} , L_{c.3} \right) = 0.0021$ $Kn_{3.2} := knudsen \left(p_t \cdot p_{3.2.to.total} , T_t \cdot T_{3.2.to.total} , L_{c.3} \right) = 0.4161$

$Kn_{5.1} := knudsen \left(p_t \cdot p_{5.1.to.total} , T_t \cdot T_{5.1.to.total} , L_{c.5} \right) = 0.0022$ $Kn_{5.2} := knudsen \left(p_t \cdot p_{5.2.to.total} , T_t \cdot T_{5.2.to.total} , L_{c.5} \right) = 0.0181$

reynolds numbers:

$Re_1 := reynolds \left(p_t , T_t , L_{c.1} , 0.001 , \gamma \right) = 1.4035$

$Re_{3.1} := reynolds \left(p_t , T_t , L_{c.3} , M_{3.1} , \gamma \right) = 0.7797$

$Re_{5.1} := reynolds \left(p_t , T_t , L_{c.5} , M_{5.1} , \gamma \right) = 0.0096$

$Re_{2.4} := reynolds \left(p_t , T_t , L_{c.2} , 1 , \gamma \right) = 0.0014$

$Re_{3.2} := reynolds \left(p_t , T_t , L_{c.3} , M_{3.2} , \gamma \right) = 0.0001$

$Re_{5.1} := reynolds \left(p_t , T_t , L_{c.5} , M_{5.2} , \gamma \right) = 0.0005$

Chapter 3.5: Disconneted Reservoirs (Isentropic):

$M_{D.iso} := \left(1 + \frac{\gamma - 1}{2} \right)^{-\frac{\gamma + 1}{2 \cdot (\gamma - 1)}} = 0.5743$

$p_{ratio} := pressure\_to\_total \left(\gamma , M_{D.iso} \right) = 0.7918$ $T_{ratio} := temp\_to\_total \left(\gamma , M_{D.iso} \right) = 0.9281$

$\rho_{ratio} := density\_to\_total \left(\gamma , M_{D.iso} \right) = 0.8531$

$m_{D.term} := massflow \left(\gamma , M_{D.iso} , A_2 , T_t , p_t \right) = 7 \cdot 10^{-8} \frac{kg}{s}$

Chapter 3.5: Disconneted Reservoirs (Isothermal):

$$f := \left(-\frac{1}{\gamma - 1} + \sqrt{\frac{1}{(\gamma - 1)^2} + \frac{2}{\gamma - 1} \cdot \left(\frac{2}{\gamma + 1}\right)^{\frac{\gamma + 1}{\gamma - 1}}} \right) = 0.3076 \qquad M_{D.term} := \sqrt{f} = 0.5546$$

$$p_{ratio} := pressure\_to\_total\left(\gamma, M_{D.term}\right) = 0.8039 \qquad T_{ratio} := temp\_to\_total\left(\gamma, M_{D.term}\right) = 0.9326$$

$$\rho_{ratio} := density\_to\_total\left(\gamma, M_{D.term}\right) = 0.862$$

$$m_{D.term} := massflow\left(\gamma, M_{D.term}, A_2, T_t, p_t\right) = 6.8468 \cdot 10^{-8} \frac{kg}{s}$$

Chapter 3.5: Formulation with leak (isentopic connection):

$$m_{L.isen}\left(A, \gamma, T_r, p_r\right) := A \cdot p_r \cdot \sqrt{\frac{\gamma}{R_s \cdot T_r}} \cdot \left(1 - \left(1 + \frac{\gamma - 1}{2}\right)^{-\frac{\gamma + 1}{2 \cdot (\gamma - 1)}}\right)$$

$$p_r := p_{crit.ratio} \cdot p_t = 0.7752 \, bar \qquad T_r := T_{crit.ratio} \cdot T_t = 404.8583 \, K$$

$$m_{L.isen}\left(A_4, \gamma, T_r, p_r\right) = 3.6258 \cdot 10^{-8} \frac{kg}{s}$$

Chapter 3.5: Formulation with leak (isothermal connection):

$$m_{L.iso}\left(A, \gamma, T, p_r\right) := A \cdot p_r \cdot \sqrt{\frac{\gamma}{R_s \cdot T}} \cdot \left(1 + \frac{\gamma - 1}{2}\right)^{-\frac{\gamma + 1}{2 \cdot (\gamma - 1)}} \cdot \left(\left(1 + \frac{\gamma - 1}{2}\right)^{\frac{\gamma}{\gamma - 1}} - 1\right)$$

$$m_{L.iso}\left(A_4, \gamma, T_r, p_r\right) = 4.5737 \cdot 10^{-8} \frac{kg}{s}$$

Chapter 3.2: expected knudsen number

Test:

$$\alpha := 0.06 \frac{Pa}{K^{\frac{3}{2}}}$$

$$Kn := knudsen\left(1 \, bar, 300 \, K, 20 \, micron\right) = 0.0034$$

$$p := \alpha \cdot \frac{T_t^{\frac{3}{2}}}{0.1} = 0.0671 \, bar$$

$$p := 1 \, bar$$

$$a := \frac{p \cdot Kn}{T_t^{\frac{3}{2}}} = 0.0021 \frac{Pa}{K^{\frac{3}{2}}}$$

Chapter 3.6: Maximum turning angle

$$\theta_{max} := \frac{\pi}{2} \cdot \left(\sqrt{\frac{\gamma + 1}{\gamma - 1}} - 1\right) - \sqrt{\frac{\gamma + 1}{\gamma - 1}} \cdot atan\left(\sqrt{\frac{\gamma - 1}{\gamma + 1} \cdot \left(M_{5.2}^2 - 1\right)}\right) + atan\left(\sqrt{M_{5.2}^2 - 1}\right) = 68.912 \, deg$$

A Calculations

A.2 Python

Packages:

- NumPy: https://numpy.org/

- SciPy: https://scipy.org/

- Pandas: https://pandas.pydata.org/

A.2.1 Solve Mach number from area ratio

Listing 1. Solve Mach number from area ratio using scipy fsolve

```python
import numpy as np
from scipy.optimize import fsolve

# Function defining the relationship between Mach number (M), area ratio
    (A/A*), and specific heat ratio (gamma)
# Used to find the Mach number given an area ratio (A/A*)
def mach_area_relation(M, A_Astar, gamma):
    return (1 / M) * ((2 / (gamma + 1)) * (1 + ((gamma - 1) / 2) * M**2))
        **((gamma + 1) / (2 * (gamma - 1))) - A_Astar

# Function to numerically solve for Mach number given an area ratio (A/A
    *), specific heat ratio (gamma), and an initial guess for Mach number
# Parameters:
# - A_Astar: Area ratio (A/A*)
# - gamma: Specific heat ratio
# - M_guess: Initial guess for Mach number (default: 1.0)
def solve_mach(A_Astar, gamma, M_guess=1.0):
    M_solution = fsolve(mach_area_relation, M_guess, args=(A_Astar, gamma
        ))
    return M_solution[0]

# Example calculation:
A_Astar = 318      # Given area ratio (A/A*)
gamma = 1.47       # Specific heat ratio for the gas

# Solve Mach number with initial guess of 0.1 (indicating expected
    subsonic solution)
M_solution = solve_mach(A_Astar, gamma, 0.1)
print(f"Solved Mach number: {M_solution:.5f}")
```

A.2.2 Dataset for Knudsen and Reynolds number plot

Listing 2. Generating data for plot of Knudsen and Reynolds numbers for different temperatures and characteristic lengths

```python
import numpy as np

# --- Constants ---
gamma = 1.47
Mm = 28.013e-3  # kg/mol (Molar mass of N2)
R_u = 8.314462618
p0 = 1.5e5

# Characteristic lengths
Lc_values = [20e-6, 40e-6]

# Stagnation temperatures
T0_values = [300.0, 600.0]
```

```python
# Viscosity model constants (Sutherland's law)
S_mu = 111.0
T_ref_mu = 300.55
mu_ref = 17.81e-6

# Mach number range (use as many points as you like)
Ma_vals = np.linspace(0.0, 3.5, 100)

def local_temperature(Ma, T0):
    return T0 / (1 + (gamma - 1) / 2 * Ma**2)

def local_pressure(Ma, p0):
    return p0 * (1 + (gamma - 1) / 2 * Ma**2) ** (-gamma / (gamma - 1))

def dynamic_viscosity(T):
    return mu_ref * (T / T_ref_mu)**1.5 * (T_ref_mu + S_mu) / (T + S_mu)

def knudsen_number(T, p, Lc):
    return (dynamic_viscosity(T) / (p * Lc)) * np.sqrt(np.pi * T * R_u /
        (2 * Mm))

def reynolds_number(Ma, Kn):
    return Ma * np.sqrt(gamma * np.pi / 2) / Kn

# We'll store columns:
#   Ma, Re(300,20µm), Re(300,40µm), Re(600,20µm), Re(600,40µm),
#       Kn(300,20µm), Kn(300,40µm), Kn(600,20µm), Kn(600,40µm)
header = "Ma  Re300_20  Re300_40  Re600_20  Re600_40  Kn300_20  Kn300_40
    Kn600_20  Kn600_40"

with open("knre_data.dat", "w") as f:
    f.write(header + "\n")
    for Ma in Ma_vals:
        # Compute for each (T0, Lc) in a fixed order
        row_data = [Ma]
        re_data = []
        kn_data = []
        # First gather Re in the order: (300,20), (300,40), (600,20),
            (600,40)
        for T0 in T0_values:
            for Lc in Lc_values:
                T = local_temperature(Ma, T0)
                p = local_pressure(Ma, p0)
                Kn = knudsen_number(T, p, Lc)
                Re = reynolds_number(Ma, Kn)
                re_data.append(Re)
        # Then gather Kn in the same parameter order
        for T0 in T0_values:
            for Lc in Lc_values:
                T = local_temperature(Ma, T0)
                p = local_pressure(Ma, p0)
                Kn = knudsen_number(T, p, Lc)
                kn_data.append(Kn)

        row_data.extend(re_data + kn_data)
        line = " ".join(f"{val:.6g}" for val in row_data)
        f.write(line + "\n")

print("Wrote knre_data.dat with columns:\n" + header)
```

B Flow Field Solution

This graph is directly copied and redrawn from the studies of Cassanova [23]: